Temperature and fire controls on vegetation dynamics in Northern Ural (Russia) boreal forests during the Holocene based on brGDGT and pollen data

Chéïma Barhoumi, Guillemette Ménot, Sébastien Joannin, Adam Ali, Salomé Ansanay-Alex, Yulia Golubeva, Dmitry Subetto, Alexander Kryshen, Igor Drobyshev, Odile Peyron

Temperature and fire controls on vegetation dynamics in Northern Ural (Russia) boreal forests during the Holocene based on brGDGT and pollen data

Chéïma Barhoumi[1], Guillemette Ménot[2], Sébastien Joannin[3], Adam A. Ali[3], Salomé Ansanay-Alex[2], Yulia Golubeva[4], Dmitry Subetto[5, 6, 7], Alexander Kryshen[8], Igor Drobyshev[9, 10] and Odile Peyron[3]

[1]Department of Palynology and Climate Dynamics, Albrecht-von-Haller Institute for Plant Sciences, University of Göttingen, Germany

[2] University of Lyon, ENS de Lyon, Univ Lyon 1, CNRS, LGL-TPE, Lyon, France

[3]Institut des Sciences de l'Evolution de Montpellier, Université de Montpellier, CNRS, IRD, EPHE, Montpellier, France

[4]Institute of Geology of the Komi Science Centre, Russian Academy of Sciences, Syktyvkar, Russia

[5]Herzen State Pedagogical University of Russia, Saint Petersburg, Russia

[6]Northern Water Problem Institute of the Karelian Research Centre of Russian Academy of Sciences, Petrozavodsk, Russia

[7]Institute for Water and Environmental Problems of the Siberian Branch of the Russian Academy of Sciences, Barnaul, Russia

[8]Forest Research Institute of the Karelian Research Centre of Russian Academy of Sciences, Petrozavodsk, Russia

[9]Southern Swedish Research Center, Swedish University of Agricultural Sciences, Alnap, Sweden

[10]Institut de recherche sur les forêts, Université du Québec en Abitibi-Témiscamingue, Québec, Canada

Corresponding author: cheima.barhoumi@gmail.com

Abstract

Boreal vegetation is influenced by multiple factors such as climate and fire, but interactions between long- and short-term effects of climate upon fire activity are complex and remain poorly studied, especially in Eurasia. To understand the relationships between climate, fire and vegetation in Eurasia, we reconstruct the climate changes during the Holocene for the western section of the Northern Urals region, in the southern part of the Republic of Komi. We relate these temperature reconstructions to pollen and charcoal records from the same region (Yaksha site, Republic of Komi, Russia). We use here a combined approach based on pollen and molecular biomarkers (branched Glycerol Dialkyl Glycerol Tetraethers or brGDGTs) to provide independent estimates of past temperatures. Our objectives were: (1) to understand the relationships between climate, fire, vegetation and human activity during the Holocene at the local scale of Yaksha and (2) to provide a robust regional-scale climatic reconstruction of the southern part of the Republic of Komi. Our study shows that climate had a major influence on the regional vegetation between 10,000 and 4000 cal. yr BP. Subsequently, fire activity had a joint and growing impact on vegetation dynamics between 4000 and 600 cal. yr BP. Finally, from 600 until the present (2016 AD), human presence and activities had a greater impact on the fire regime and vegetation than earlier in time, and combined with climate to influence the dynamics of the boreal forest. At the regional scale of the Republic of Komi and the local scale of Yaksha, the Holocene Thermal Maximum was detected between 6800 and 4000 cal. yr BP, using pollen-based temperature estimates but in brGDGT calibration (at 4000 cal. yr BP) commonly shared in the literature, together with evidence from neighboring regions in the Eurasian boreal biome which were studied for different proxies (pollen, chironomids), and also with reference to climate models (General Circulation Models).

Keywords: brGDGT; Pollen; Quantitative climate reconstructions; Holocene; Republic of Komi, Northern Urals, boreal forests, fire histories

1. Introduction

Boreal regions are among the most sensitive regions to current and future climate change (IPCC-AR6, Pörtner *et al.*, 2022). Climate influences boreal biomes through direct control of the biomass accumulation rates and shapes natural disturbance regimes such as wildfires. General Circulation Models (GCMs) integrating these effects, suggest that the circumboreal zone will shrink by 2071-2100 (Feng et al., 2014). The simulated decline of the boreal biome is attributed to a precipitation increase (especially in winter), and a temperature increase (between +6° and +8°C), driving an increase in fire activity (Goetz *et al.*, 2007; de Groot *et al.*, 2013; Feng *et al.*, 2014; Hoegh-Guldberg *et al.*, 2018).

Climate and fire are the main drivers of vegetation, but interactions between them are complex and poorly studied in Eurasian boreal forests (Glückler et al., 2020; Goldammer and Furyaev, 1996; Kharuk et al., 2021). Climate impacts fire frequency, fire severity and burned area. An increase in fire activity likely increases the share of serotinous tree species such as *Betula pendula* Roth., *B. pubescens* Ehrh. (hereafter *Betula* spp.) and *Pinus sylvestris* L. (hereafter *Pinus sylvestris)* (de Groot et al., 2013; Goetz et al., 2007). In contrast, enhanced summer precipitation counteracts this effect and favors *Picea abies* (L.) H.Karst. (hereafter *Picea abies*) and *Pinus sibirica Du Tour* (hereafter *Pinus sibirica)* (Feng *et al.*, 2014; Hoegh-Guldberg *et al.*, 2018). In North American boreal forests, fire events were found to be influenced by climate and human activity, but also by the type of vegetation (eg Ali et al., 2012; Camill et al., 2009; Girardin et al., 2013; Hu et al., 2006; Remy et al., 2017). For example, in Canada, during the Mid-Holocene (6000 cal. yr BP), forest dominated by boreal mixed woodland vegetation was associated with low fire frequency, while the climate was warm and dry. But from 3000 cal. yr BP, despite colder and wetter conditions, fire frequency increased, because of the vegetation shift toward a dense needleleaf landscape (Girardin et al., 2013).

Recent regional climate synthesis studies have pointed out specific regional patterns of climate variability during the Holocene period (Kaufman et al., 2020; Marcott et al., 2013; Marsicek et al., 2018; Mauri et al., 2015; Herzschuh et al., 2022). In Europe, the climate synthesis by Kaufman et al., (2020) based on various proxies such as pollen, chironomids, and molecular biomarkers, indicated a warming trend in the Northern latitudes during the Early Holocene followed by a cooling since 6000 yr BP. This study also showed that the climate patterns are proxy-specific. For example, the temperature optimum was recorded at 10,000 years BP from reconstructions based on chironomids and at 6000 years BP from reconstructions based on pollen (Kaufman et al., 2020). The climate synthesis by Herzschuh et al. (2022) based on pollen data only, also indicate a temperature optimum between 8000 to 6000 yrs cal BP, but the timing and the amplitude of this optimum is strongly dependent on latitude, and appears more marked at high latitudes (70 to 80 °N) and less marked between 60 to 70°N. These global syntheses also highlight the poor “past climate” coverage of Eurasia and particularly of Russia, despite their geographical extent and role in global biochemical cycles. The general lack

of data is particularly apparent in the Republic of Komi, West of the Northern Urals area (Golubeva, 2008), despite its climatic relevance, at the confluence of several atmospheric meteorological mechanisms (Ural Blocking, Siberian High, Arctic Oscillations) (Wang et al., 2010; Dole et al., 2011; Cheung et al., 2012; H. Cheung and Zhou, 2015). Our earlier investigations of pollen and charcoal records in the Republic of Komi, in the Yaksha area, revealed a shift in the boreal forest tree species as well as increasing fire activity during the Holocene (Barhoumi et al., 2020, 2019). However, the role of climate in the interactions between fire and vegetation has not yet been well documented. The only study of Holocene climate in this area reconstructs increasing temperatures between 6000 and 4800 cal. yr BP (Golubeva, 2008). In the neighboring sub-regions of Northern Europe and Fennoscandia, several studies based on pollen and chironomids indicate an increase in temperatures between 8000 and 3500 cal. yr BP (e.g. Seppä *et al.*, 2009; Salonen *et al.*, 2011). On the eastern side of the Urals, some studies of the Holocene climate have been carried out in the Taymyr peninsula (Andreev et al., 2002; Velichko et al., 2002). These studies suggest that in the Early Holocene (between 10,300 and 9000 cal. yr BP), temperatures were slightly cooler (-1 °C) than today, but wetter (+ 50 mm precipitation compared to present). At the Entarny site (Velichko et al., 2002), the Early Holocene also showed colder temperatures (-2.5 °C), but also less precipitation (- 25 mm compared to today). The main studies of Holocene climate-vegetation-fire relationships in the east of the Republic of Komi were carried out in Siberia, around Lake Baikal (Barhoumi et al., 2021; Bezrukova et al., 2013, 2003; Demske et al., 2005; Feng et al., 2014; Tarasov et al., 2007, 2009). According to these studies, from the Early Holocene to the Mid-Holocene (11,000-8000 cal. yr BP), conditions were colder and wetter. From 8000 to 5000 cal. yr BP, the Lake Baikal region experienced its climatic optimum with wet conditions. From 5000 to 3000 cal. yr BP temperatures and precipitation decreased before increasing again from 3000 to the present day. Most of these studies are based on pollen records and transfer functions (eg Chevalier *et al.*, 2020) and vegetation-independent studies are needed to provide more reliable climate reconstructions.

With this study, we reconstruct Holocene temperature and precipitation patterns in the Republic of Komi using a coupled approach including pollen data and organic biomarkers Glycerol Dialkyl Glycerol Tetraethers (GDGTs) (Dugerdil et al., 2021; Martin et al., 2020; Ramos-Román et al., 2022; Robles et al., 2022). GDGTs are membrane lipid molecules of bacterial origin (Damsté et al., 2000; Weijers et al., 2006b), ubiquitously found in oceans, lakes and rivers, peats and soils. GDGT distributions in these environments broadly correlate to mean annual temperatures and pH (e.g. Weijers et al., 2007a; Petersee et al., 2010). Different calibrations were performed on soils, lake sediments and peatlands to infer temperatures for GDGTs and more specifically brGDGTs (branched-GDGTs, Damsté *et al.*, 2000; Weijers, Schouten, van den Donker, *et al.*, 2007; Weijers, Schouten, Sluijs, *et al.*, 2007; Peterse *et al.*, 2012; Foster *et al.*, 2016; Naafs *et al.*, 2017; Dearing Crampton-Flood *et al.*, 2020). To our knowledge, there are very few Holocene temperature reconstructions based on pollen grains and brGDGTs, which are independent climate

proxies (Dugerdil et al., 2021; Martin et al., 2020; Ramos-Román et al., 2022; Robles et al., 2022), and the brGDGT calibrations have never been used to reconstruct Holocene temperatures in Russia.

The objective of this study is first to understand the links between climate, fire regime, vegetation dynamics and human activity over the Holocene at the local scale of the Yaksha area, and secondly, to provide a robust reconstruction of the climate changes during the Holocene in the southern part of the Republic of Komi, in the Northern Urals area. Temperature reconstructions for Yaksha are based on two independent proxies, pollen and brGDGT. They are discussed in relation to the dynamics of both fire regimes and forest vegetation reconstructed from charcoal and pollen by Barhoumi *et al.*, (2019, 2020). We provide a regional perspective on the climate trends through the Holocene by applying the same pollen transfer functions to the other pollen records available from the area. Finally, we compare our results with climate reconstructions developed for Northern Europe and neighboring regions.

2. Material and Methods

2.1 Environmental setting of the study area

European boreal forests are constituted of patches of "light taiga" forests type dominated by *Pinus sylvestris*, *Larix sibirica* Ledeb. (hereafter *Larix sibirica*) and *Betula* sp, associated with a surface fire regime in drier environments, and the "dark taiga" forests type, in wetter environments dominated by *Picea abies*, *Pinus sibirica*, and *Abies sibirica*, where crown fires can occur (Goldammer, 2015; Lapenis et al., 2005; Schulze et al., 2005; Shorohova et al., 2009). In the western part of the Northern Urals, the boreal vegetation is dominated by *Larix sibirica* and *Pinus* sp.

Yaksha. One of the study sites (Fig. 1, Table 1), is a forested peatbog of 4 hectares located in the south of the Republic of Komi (Barhoumi et al., 2019, 2020). The Republic of Komi (Fig. 1) is a Russian administrative division of 415 900 km2, occupying the western side of the Ural Mountains. The soils of the region are mainly moraine and surface loams (Drobyshev et al., 2004a; Zaboeva, 1997), with podzolic soils and the topography is flat except near the Ural Mountains (Naryshkin, 2003).

The local forest cover (assessed within a 10 km radius around the Yaksha site) consists today mainly of Scots pines (*Pinus sylvestris*, 84%), spruce (*Picea abies*, 13%) and birch (*Betula pendula* and *B. pubescens*, 2%). In contrast, spruce forests dominate regionally.

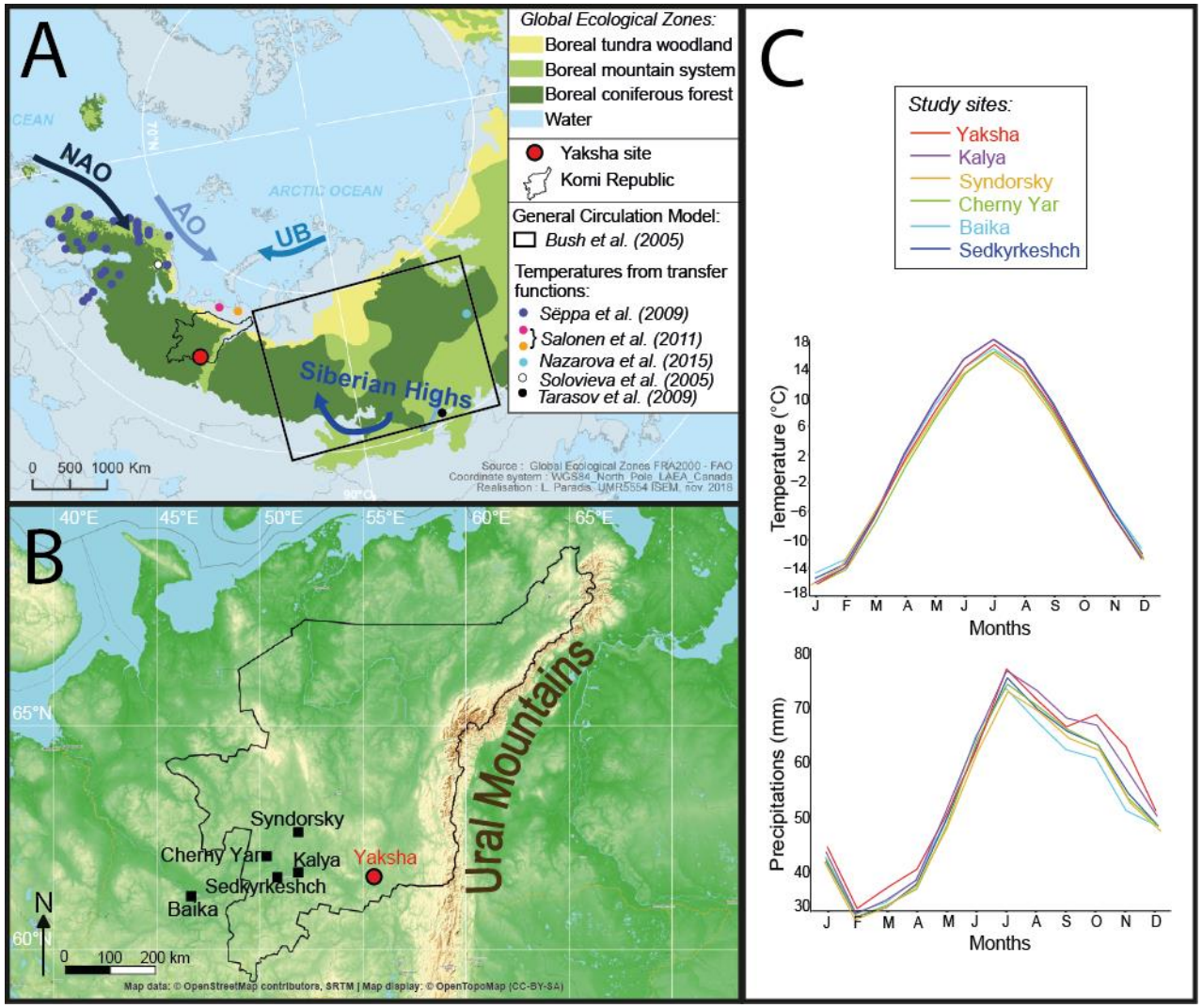

110

111 *Figure 1 :* ***A****: The Republic of Komi in the Eurasian boreal biome (highlighted black contours). Location of the Yaksha coring site (red dot) as*
112 *well as available temperature reconstructions cited in the text ((colored dots Solovieva, Tarasov and MacDonald, 2005; Seppä* et al.*, 2009;*
113 *Tarasov, Bezrukova and Krivonogov, 2009; Salonen* et al.*, 2011; Nazarova* et al.*, 2015a; Novenko and Olchev, 2015; Druzhinina* et al.*, 2020).*
114 *The black square corresponds to the zone for which climate outputs are available from the General Circulation Model GFDL (Bush, 2005), UB:*
115 *Ural Blocking; AO: Arctic Oscillations; NAO: North Atlantic Oscillations.* ***B****: The Republic of Komi and the pollen records used for the Holocene*
116 *climate regional synthesis (Yaksha – this study, Kalya, Syndorsky, Cherny Yar, Baika and Sedkyrkeshch (Borisova, 2002), Sedkyrkeshch*
117 *(Golubeva, 2008), Kalya (Karmanov et al., 2011), Cherny Yar (Marchenko-Vagapova and Marieva, 2001) and Syndorsky (Golubeva, 2008)).* ***C****:*
118 *Ombrothermic diagrams of each studied site (Grieser et al., 2006).*

119

120 In the Northern Urals region in Republic of Komi, a blocking, which is an anticyclonic or cyclonic vortex on a large scale and which remains
121 quasi stationary, takes place (Ural Blocking, UB or also so-called Ural-Siberian Blocking, USB) (Cheung et al., 2013, 2012). UB (Fig. 1A) is
122 generally more active and intense during boreal winter, acting as a barrier to Siberian Highs during this period, but amplifying its effect on the
123 east-Asian sub-continent and causing harsher winters (Wang *et al.*, 2010; Cheung *et al.*, 2013; Cheung and Zhou, 2015). The intensity of UB

during winter is also linked to the phases of the Arctic Oscillation (AO) (Cheung et al., 2012). On the other hand, Rossby waves, another atmospheric phenomena, occur and have an impact on the climate of Europe and Western Russia (Dole et al., 2011; Schubert et al., 2011, 2014). For example, during summer 2010, strong heat waves occurred and had direct effects on wildfire activity in the Ural Mountains (Cheung et al., 2013; Dole et al., 2011; Lau and Kim, 2012; Matsueda, 2011). In the study area, a UB occurring during the NAO positive phase may lead to a regional warming in the atmospheric winter temperatures (Huang et al., 2017).

In the North of the Republic of Komi, the mean annual temperature is -6°C, while it is +1°C in the South (Figure 1C). Annual precipitation varies between 450 and 700 mm (Drobyshev et al., 2004b; Grieser et al., 2006) (Figure 1C).

2.2 Study sites and material

We extracted two peat cores (Yak2-A and Yak3-A) using an 8-cm diameter Russian peat corer from the centers of the selected *Sphagnum* peatlands. We built a composite sequence from the two cores Yak2-A and Yak3-A to obtain the longest chronology (Barhoumi et al., 2019, 2020). The 0 to 300 cm interval of core Yak3-A provided the best temporal resolution of the Yaksha composite core. Although having a lower temporal resolution than Yak3-A, the deeper part of core Yak2-A is constituted of organic-rich sediments reaching 11,000 cal. yr BP (Barhoumi et al., 2019). The chronology was based on 12 radiocarbon dates, with the age model discussed in detail in Barhoumi et al. (2019) (see Appendix SI 1). The Yaksha core provided both a charcoal record (Barhoumi et al., 2019) and a pollen record (Barhoumi et al., 2020). This study focuses on the pollen-inferred climate reconstruction, the brGDGT analysis and the brGDGT-inferred temperature reconstruction.

We also benefited from five published pollen sequences (Fig. 1B, Table 1) located close to the Yaksha site to reconstruct the climate in the area during the Holocene. From South to North, these pollen sequences were Baika (Borisova, 2002), Sedkyrkeshch (Golubeva, 2008), Kalya (Karmanov et al., 2011), Cherny Yar (Marchenko-Vagapova and Marieva, 2001) and Syndorsky (Golubeva, 2008). Modern values for annual temperatures and precipitation were established with the software New_Locclim (Grieser et al., 2006), a local climate estimator using the updated FAOCLIM database (https://www.faoswalim.org). The 2010-2018 meteorological records for the coordinates of these sites, from the Worldclim database, at a spatial resolution of 2.5 minutes, were used to verify the correlation between the mean annual temperatures, the mean summer temperatures (June, July, August, corresponding to the fire season) and the mean temperatures of the months above 0°C (from April to October) (Fick and Hijmans, 2017; Harris et al., 2014).

Table 1: Pollen records selected for the climate reconstruction synthesis

Name of the site	**Coordinates**	**Elevation (a. s. l. in m)**	**Time covered (cal. yr BP)**	**References**
Yaksha	61°43'N, 55°29'E 61°41'N, 55°34'E	135	10,047 to -50	This study; Barhoumi *et al.*, 2019, 2020.
Baika	61°16'N, 46°44'E	60	8775 - 50	Borisova, 2002
Cherny Yar	62°13'N, 50°17'E	90	8532 - 2876	Marchenko-Vagapova and Marieva, 2001
Kalya	61°48'N, 51°47'E	101	10,150 - 0	Karmanov *et al.*, 2011
Sedkyrkeshch	61°43'N, 50°51'E	95	4244 - 1197	Golubeva, 2008
Syndorsky	62°44'N, 51°51'E	138	9434 - 4727	Golubeva, 2008

These pollen sequences provide a vegetation synthesis in the Southern part of the Komi Republic as follows (Appendix SI 2):

At Yaksha, from 10,000 cal. yr BP to 5000 cal. yr BP, the vegetation was dominated by *Pinus sylvestris* and *Betula spp.* This vegetation fits with the present description of a light taiga system. From 6050 BP to 100 cal. yr BP the pollen assemblages show an increase of *Picea* and the occurrence of *Pinus sibirica*, suggesting the establishment of a predominantly dark taiga. From 3200 to 100 cal. yr BP, the dark taiga decreased slowly and the light taiga reappeared, with an increase of *Pinus sylvestris*. From 100 cal. yr BP to 0 cal. yr BP, there was a strong increase in *Betula spp.*

At Kalya, close to Yaksha, vegetation changes are consistent with the Yaksha ones: in the first half of the Holocene, from 9000 to 6000, light taiga taxa were predominant. In the Mid-Holocene, *Picea abies* disappeared. Then from 5000 to 3500 cal. yr BP *Picea abies* increased again but remained less numerous than *Pinus sylvestris* and *Betula spp.* From 3500 cal. yr BP, the light taiga was predominant with *Pinus sylvestris* and *Betula spp.*

In Sedkyrkeshch, Syndorsky and Cherny Yar, pollen diagrams only cover part of the Holocene. At Sedkyrkeshch, few changes were observed between 4000 and 1000 cal. yr BP. *Betula spp.* was the main taxa. *Pinus sylvestris* and *Picea abies* were equally present. In Syndorsky, *Betula spp.* dominated in the Early Holocene (from 9000 to 6500 cal. yr BP), followed by *Pinus sylvestris* from 6500 to 5000 cal. yr BP. *Picea abies* (dark taiga) culminated around 8000 cal. yr BP. In Cherny Yar, as in Yaksha and Kalya, the first half of the Holocene showed landscapes mostly consisting of forests dominated by *Betula spp.* up to 6000 cal. yr BP. From 6000 to 3000 cal. yr BP, *Betula*-dominated forests and dark taiga (*Picea abies*) were both present.

At Baika, before 10,000 cal. yr BP, the forests had not yet significantly developed; subsequently, *Picea abies*, *Pinus sylvestris* and *Betula spp.* Forests developed. From 10,000 to 5000 cal. yr BP, dark taiga with *Picea abies* was predominant. From 5000 to 2500 cal. yr BP, *Picea abies* decreased in favor of light taiga taxa, before developing again from 2500 cal. yr BP until the present day.

2.3 Pollen-inferred climate reconstructions: a multi-method approach

The pollen-based climate reconstructions were performed using two different methods, in order to increase the reliability of our reconstruction: the Modern Analogue Technique (MAT; Guiot, 1990) and the Weighted Averaging Partial Least Squares Regression (WA-PLS; ter Braak and Juggins, 1993). Transfer functions (such as WA-PLS) and assemblage approaches (such as MAT) require a robust modern pollen calibration dataset. The MAT compares the composition of modern pollen assemblages compiled in the modern dataset with fossil pollen assemblages by calculating a chord distance (a Euclidian distance on square-root-transformed abundances) (Guiot, 1990). When the chord distance reaches a threshold value, modern pollen assemblages samples are rejected. On the other hand, the closest modern pollen samples are retained as the best analogues, and the weighted average of their climate parameters is calculated to provide the past climate estimates (where the weights used are the inverse of the chord distance) (Guiot, 1990). We chose between 6 to 8 analogues (depending on the site and the climatic parameters), using a leave-one-out cross-validation test. WA-PLS is a transfer function, a regression method that assumes that the relationships between pollen percentages and climate are unimodal, and that for each taxon there is an optimal climate variable value. With this method, the modern pollen data set used can be considered as a large multidimensional matrix. Since there is collinearity between pollen taxa, and since some taxa are linked to the climatic parameters of interest, it is possible to resize the dataset to a reduced number of components based on the linear predictors of the parameter of interest and on the residual structure of the data when these predictors are removed (Peyron et al., 2013).

The modern dataset used here for the Yaksha and other sequences climate reconstructions was a sub-dataset from a Eurasian database (Peyron et al., 2005), with more than 3000 sites (Peyron et al., 2008; Dugerdil et al., 2021). The sub-dataset selected here includes 2115 sites located mainly in Russia but also in Northern and Central Europe. We chose to constrain the original dataset to increase the robustness of the climatic parameter reconstruction. With that objective, we selected biomes comparable to the climate and ecosystems in the region of the Republic of Komi. The sites corresponding to the biomes Cold Deciduous Forest, Cold Mixed Forest, Cold Coniferous Forest, Cold Steppe, Pioneer Environments, Taiga forest and Tundra (Peyron et al., 1998; Prentice et al., 1996) were selected in the sub-dataset.

The R package 'Rioja' was used to reconstruct the past climate parameters with both methods (Juggins, 2009; Juggins and Juggins, 2020). Climate parameters are: mean annual temperatures (TANN) and annual precipitation (PANN), mean summer temperatures (MTWA) and summer precipitation (SUMMERPR). The performance of the two methods was tested on the database by randomly using 60% of it to calibrate and the remaining 40% to test the transfer functions. The same test was carried out by selecting the 19 samples from the database between latitudes 40 and 50°N and longitudes 40 and 50°E, representing the closest samples from the database to the Yaksha site. The correlations between the reconstructed values and the observed values of the database are presented in Appendix SI 3 and SI 4. A redundancy analysis (RDA) was performed to compare the main pollen taxa (*Betula* spp., *Pinus sylvestris*, *Pinus sibirica*, *Picea abies*, *Abies sibirica* and Other taxa) with reconstructed climate parameters inferred from pollen MAT (TANN, PANN, MTWA and SUMMERPR), fire activity (mFRI) and human population density. The fire activity data come from Barhoumi et al. (2020, 2019) who calculated and computed temporally the mean Fire Return Interval of Yaksha study site. The human population density numerical data come from the HYDE 3.1 database (Klein Goldewijk et al., 2011) and were downloaded here: https://landuse.sites.uu.nl/datasets/.

2.4 GDGT analysis

Key samples representative of the sedimentary sequences and the lithologic transitions were processed for GDGT analyses at ENS de Lyon (LGLTPE, France): 26 and 12 from Yak3-A and Yak2-A, respectively. Samples were freeze-dried and grounded. To aliquots of less than a gram, a C_{46} GDGT standard solution, at 10 ng.µL^{-1} was added (Huguet et al., 2006). Then, lipids were microwaved (MARS, CEM) with dichloromethane (DCM):MeOH (3:1). Total lipid extracts were separated into polar and apolar fractions on an Al_2O_3 column (1 g) with hexane:DCM (1:1) and DCM/MeOH (1:1). The separated fractions were then analyzed using a High Performance Liquid Chromatography Mass Spectrometer (HPLC-MS, Agilent 1200) (Hopmans et al., 2016; Davtian et al., 2018). The detected peak signals were integrated on the Agilent, LC/MS Chemstation Software. Branched-GDGT compositions (brGDGTs, Damsté *et al.*, 2000; Weijers, Schouten, Sluijs *et al.*, 2007, 2007) were quantified.

The reproducibility and stability of the analytical process was assessed through regular chemistry and analysis of an internal standard peat sample. Reproducibility of the measurements was calculated by replicate analyses of two contrasted samples of the sediment core.

2.5 GDGT indices and temperature reconstructions

BrGDGTs (see compound shape in Figure 1 from Naafs *et al*., 2018) are distinguished by the proportions of tetra- (I), penta- (II) and hexa- (III) methylated forms and by the number of cyclopentane moieties, which can be 0 (a), 1 (b), or 2 (c). brGDGT fractional abundances were combined into several indices (Table 2) such as the Branched and Isoprenoid Tetraether Index (BIT - Hopmans *et al.*, 2004), the IIIa/IIa ratio (Xiao et al., 2016), in which we included the 5/6 and 7-Methyled form, the Cyclization ratio of Branched Tetraethers (CBT - Weijers *et al.*, 2007a) and the Methylation of Branched Tetraether (MBT'- Peterse *et al.*, 2012 and MBT'$_{5Me}$ - De Jonge *et al.*, 2014b).

Table 2: Indices and temperature calibrations based on brGDGT fractional abundances

Indices/Temperature calibrations	**Formula or model**	**References**
CBT	$= -log\left(\frac{Ib + IIb + IIb6Me}{Ia + IIa + IIa6Me}\right)$	(Weijers et al., 2007b)
MBT'	$= \frac{I\,a + I\,b + I\,c}{Ia + Ib + Ic + IIa' + IIa'' + IIa7Me + IIb' + IIb'' + IIc' + IIc'' + IIIa' + IIIa'' + IIIb' + IIIb'' + IIIc'}$	(Peterse et al., 2012)
MBT'$_{5Me}$	$= \frac{Ia + Ib + Ic}{Ia + Ib + Ic + IIa + IIb + IIc + IIIa}$	(De Jonge et al., 2014)
CI	$= \frac{Ia}{Ia + IIa + IIIa}$	(De Jonge et al., 2019)
MAT$_{Peterse}$	$= 0.81 - 5.67 \times CBT + 31.0 \times MBT'$	(Peterse et al., 2012)
MAT$_{Naafs}$	$= 52.18 \times MBT'5Me - 23.05$	(Naafs et al., 2017)
MAT$_{Crampton\text{-}Flood}$	*Bayesian regression model (BayMBT0, for mean annual temperatures above zero)*	(Dearing Crampton-Flood et al., 2020)
MST$_{Foster}$	$= 18.7 + (80 \times Ib) - (23.05 \times II) - (19.4 \times III) + (369.9 \times IIIb)$	(Foster et al., 2016)

Temperature reconstructions were based upon several indices, including the Methyl Index of Branched Tetraether (MBT - (Weijers et al., 2007b). This has been modified by Peterse *et al*. (2012) to yield MBT', and by Naafs *et al*. (2017) to give MBT'$_{5Me,}$ excluding brGDGT 6-methyl. We tested four calibration equations and models, assessed on global datasets of soils and peats. This allowed us to derive Mean Annual Air Temperature (hereafter called MAT$_{Peterse}$ and MAT$_{Naafs}$), Mean Annual Temperature above 0°C (herafter called MAT$_{Crampton\text{-}Flood}$) and Mean Summer Air Temperature (hereafter called MST$_{Foster}$). These calibrations are respectively based on Peterse *et al.* (2012), Naafs *et al.* (2017), Dearing Crampton-Flood *et al.*, (2020) and Foster *et al.*, (2016).

3. Results

3.1 Pollen-inferred climate patterns

The mean annual temperatures (TANN) and annual precipitation (PANN) of the Yaksha, Kalya, Baika and Cherny Yar sites are presented in Fig. 2. The two other sites (Sedkyrkeshch and Syndorsky), which cover only a small part of the Holocene, are presented in Appendix SI 5, as well as mean summer temperatures (MTWA) and summer precipitation for each site.

During the Holocene, the mean annual temperatures reconstructed using the Modern Analogue Technique and the Weighted Averaging Partial Least Squares Regression, from the different cores (Yaksha, Kalya, Baika, Cherny Yar) were broadly similar in terms of trends and amplitudes (Fig. 2). In Yaksha, Kalya and Baika, the temperature values reconstructed from the most recent samples were very close to the measured modern values (-0.37°C at Yaksha, +0.39°C at Kalya and +1.46°C at Baika). From 10,000 to 7000 cal. yr BP, higher than present day temperatures were reconstructed for Yaksha and Baika (+3 °C). At Kalya, however, the temperature trends reconstructed with the two methods were similar only from 5500 to 0 cal. yr BP (Fig. 2). Noteably, the climate reconstruction began from 9000 cal. yr BP with lower values than today and the temperature increased until 7000 cal. yr BP. Yaksha, Kalya and Baika records show a Holocene Thermal Maximum (HTM) extending between 6800 cal. yr BP and 4000 cal. yr BP, with temperature values from +1°C (MAT) to +3°C (WA-PLS) relative to the present. From 4000 to 3000 cal. yr BP, the results show a general decrease in temperatures, with values lower than today (Yaksha) or very close to modern values (Baika and Kalya). Then, from 3000 to 0 cal. yr BP, the temperatures rose gradually and reach current values.

Mean annual precipitation (PANN) estimates at Yaksha show differences between the two methods but for Kalya, Baika and Cherny Yar, the precipitation reconstructions were very similar for MAT and WA-PLS (Fig. 2). For all these sites (except Baika), there was a general increase in precipitation during the Holocene. At the onset of the Holocene, between 10,000 and 8000 cal. yr BP, Yaksha and Kalya show precipitation values slightly below the modern values (about 630 mm/year, especially with MAT results). Baika recorded a decrease of precipitation from 9000 to 8000 cal. yr BP. Then, from 8000 to 5000 cal. yr BP, the PANN at Baika shows an increasing trend, as do all the other sites. From 5000 cal. yr BP, a precipitation decrease was observed (WA-PLS at Yaksha), up to about 3500 cal. yr BP. From 3500 cal. yr BP, PANN stabilized at modern values for Yaksha (WA-PLS) and Baika. They increased up to 1500 cal. yr BP in Kalya, before gradually decreasing to the later values up to the present day.

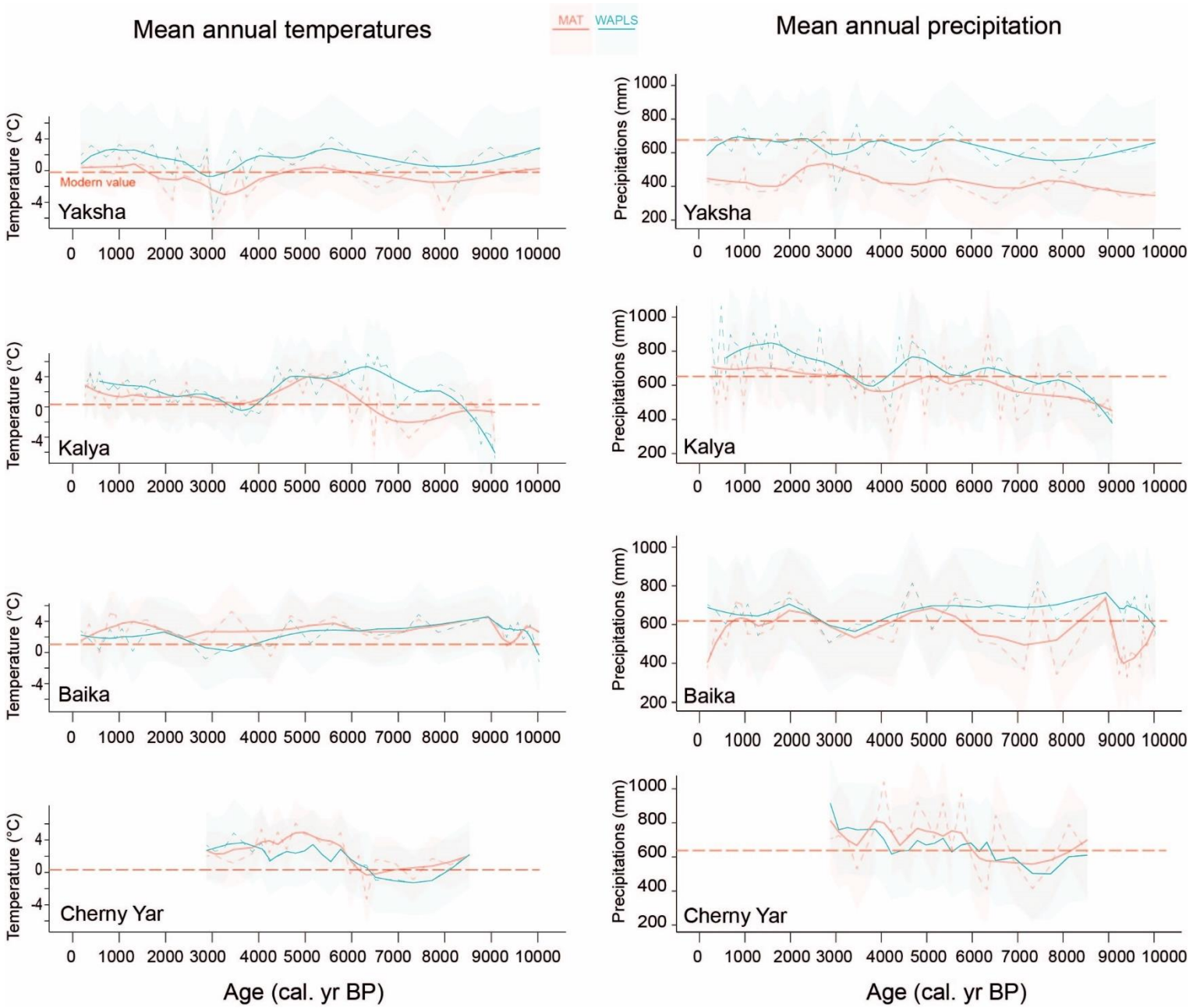

Figure 2: Regional climatic synthesis for the Republic of Komi from pollen-based reconstructions. Mean annual temperature and mean annual precipitation (dashed lines) were calculated with the Modern Analogue technique (MAT) and the Weighted Averaging Partial Least Squares Regression (WA-PLS) and smoothed with Loess (span = 0.3, solid lines). Shaded areas are confidence interval. Red dashed lines are modern values for each site.

3.2 GDGT abundances and indices

Within the Yaksha record, the majority of brGDGTs are tetramethylated Ia (48%) and pentamethylated forms IIa (39%) (Fig. 3A). The hexamethylated form IIIa represents 6% of the total brGDGTs. The remaining brGDGTs are present at values below 2%. The GDGT signatures from Yaksha were similar to those in the global database (Naafs *et al.*, 2017) and were charactersitic of mid- and high-latitude sites (Fig. 3B).

The average BIT index is 0.998 ± 0.005. The MBT'$_{5Me}$ and MBT' signals (used to infer temperature) vary little along the core (Fig. 3C), but show the lowest values (0.39 - 0.4) between 4740 and 5580 cal. yr BP and at 8980 cal. yr BP. The maximum value of 0.64 is at 4020 cal. yr BP. CI (Community Index, Table 2, De Jonge et al., 2019) shows the same variations as the MBT'$_{5Me}$ and MBT' signals and values similar to those of MBT'$_{5Me}$. These indices show high values at the very beginning of the Holocene, from 10,000 to about 9200 cal. yr BP. There are also high values between 8600 and 6500 cal. yr BP, and again between 4500 cal. yr BP. until the end of the record. PCA of Yaksha brGDGTs was performed (see SI 6). The eigenvalues of the first 2 axes of this PCA are presented in Fig. 3D (axis 1) and 3E (axis 2). Outlier brGDGT samples were highlighted by cutoff values of 1 (for axis 1) and 2 (for axis 2).

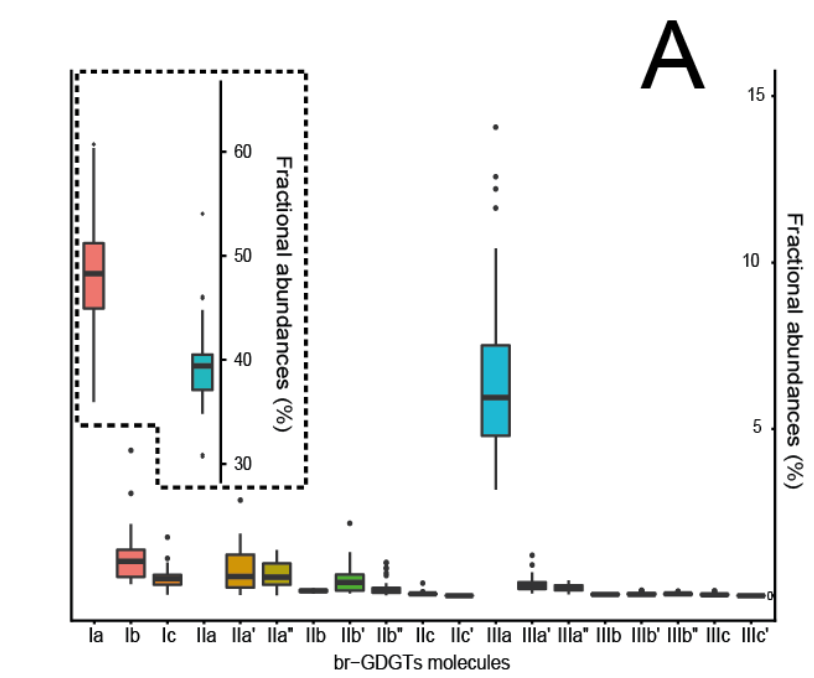
A
Fractional abundances (%)
Fractional abundances (%)
Ia Ib Ic IIa IIa' IIa" IIb IIb' IIb" IIc IIc' IIIa IIIa' IIIa" IIIb IIIb' IIIb" IIIc IIIc'
br−GDGTs molecules

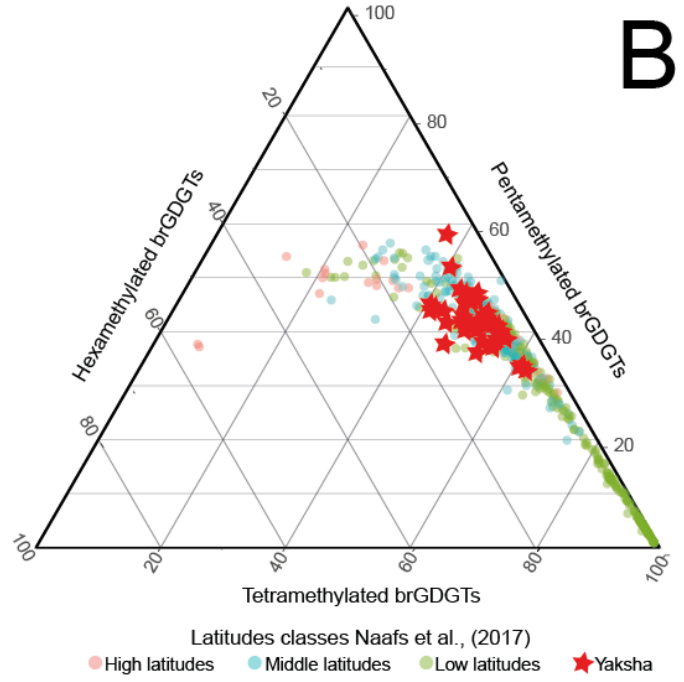
B
Hexamethylated brGDGTs
Pentamethylated brGDGTs
Tetramethylated brGDGTs
Latitudes classes Naafs et al., (2017)
High latitudes
Middle latitudes
Low latitudes
Yaksha

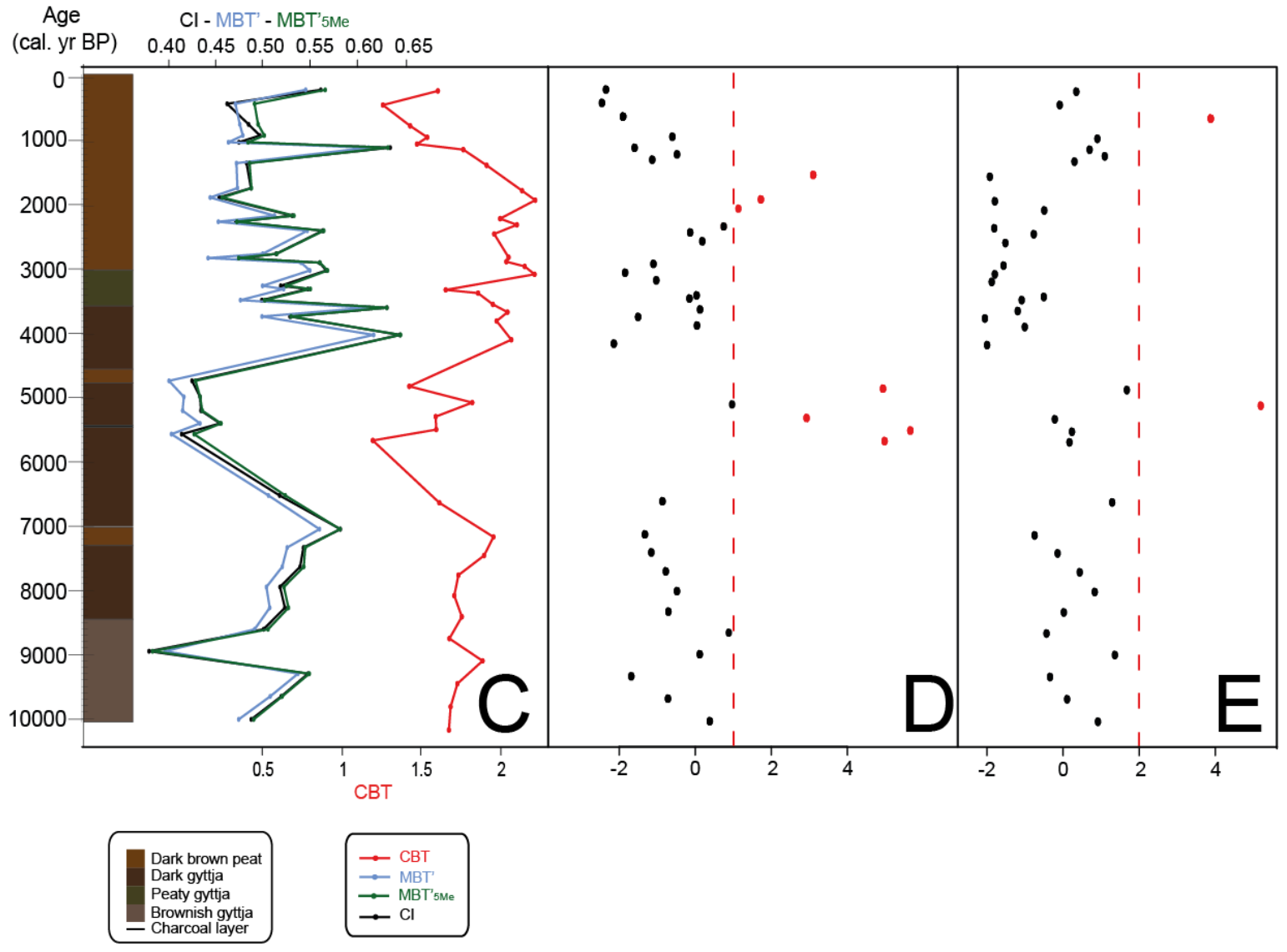
Age
(cal. yr BP)
CI - MBT' - MBT'5Me
CBT
C
D
E
Dark brown peat
Dark gyttja
Peaty gyttja
Brownish gyttja
Charcoal layer
CBT
MBT'
MBT'5Me
CI

*Figure 3: **A**: brGDGT fractional abundances in the Yaksha sequence measurement represented against two % scales. B: Ternary plot of the relative abundances of tetra-, penta-, and hexamethylated brGDGTs compared to the general database from Naafs* et al. *(2017) sorted by latitude classes. **C**: CBT, CI, MBT' and MBT'$_{5Me}$ indices. **D** and **E**: Individual PCA eigenvalues according to axis 1 (D) and axis 2 (E). Red dots are samples above the threshold separating main samples from outlier points*

4. Discussion

4.1 Yaksha local temperature reconstructions: brGDGT and pollen comparison

4.1.1 brGDGT origins

The brGDGT signal from the Yaksha study site is consistent with a terrigenous origin: the BIT index remains very close to 1 throughout the sediment core (Hopmans et al., 2004).

BrGDGT forms without cyclopentane moieties, Ia and IIa, are the main compounds within the Yaksha sedimentary core (Fig. 3A). This agrees with several studies on brGDGTs from soils and peatlands (Li et al., 2017; Loomis et al., 2014; Sun et al., 2011; Weijers et al., 2010, 2007b, 2006a, 2006b). This observation also confirms that the production of Yaksha brGDGTs is mainly of terrigenous origin since *in situ* production contains more methyl groups and cycle forms (Loomis et al., 2014; Tierney et al., 2012, 2010). Form IIIa, which is the third most abundant brGDGT compound here, is therefore likely to have come from the small amount which would have been produced *in situ*, when the peatland was submerged (Buckles et al., 2014; Cao et al., 2017; Loomis et al., 2014, 2011; Tierney et al., 2010). The variations in CI appear to coincide with the sample outliers indicated by the PCA eigenvalues of the brGDGTs samples. This could indicate a shift in brGDGT-producer communities, since they may respond differently to varying atmospheric temperatures (De Jonge et al., 2019). These samples (at 400 cal. yr BP ; from 1330 to 1870 cal. yr BP and from 4740 to 5580 cal. yr BP) were therefore not considered in the discussion and interpretation of the results of the temperature calibrations.

Moreover, peatland is an environment in which one part (catotelm) is anoxic and constantly saturated with water, while another part (acrotelm) contains living *Sphagna* and exhibits large variability in oxygen content. Studies have shown that the concentration of brGDGTs is significantly higher in catotelm than in acrotelm (Weijers et al., 2004). This differentiates the dynamics of brGDGT communities depending on the nature of the sediment through the core and has an impact on reconstruction of the annual air temperatures. For this reason we tested four calibrations, one

for soil environments, $MAT_{Peterse}$ (Peterse et al., 2012), and two specific to peatland environments, MAT_{Naafs} and $MAT_{Crampton\text{-}Flood}$, (Dearing Crampton-Flood et al., 2020; Naafs et al., 2017). We tested another calibration, reconstructing summer temperatures or temperatures of the months above 0°C, regionally adapted for Antarctic and sub-Antarctic lakes, MST_{Foster} (Foster et al., 2016), which is close to the climate of the Republic of Komi. (Fig. 4).

4.1.2 brGDGT calibration for mean annual temperatures reconstruction

The brGDGT reconstructed temperatures (Fig. 4) ranged between: $MAT_{Peterse}$: +2.5 to +10.5°C, MST_{Foster}: +5.5 to +9.9°C, MAT_{Naafs}: -3 to +10.6°C and $MAT_{Crampton\text{-}Flood}$: +5.2 to +14.1°C. The four calibrations show similar patterns. The first half of the Holocene, from 10,000 to 6500 cal. yr BP, shows a steady increase of the temperatures (+2°C). Then, from 4000 cal. yr BP to 2100 cal. yr BP, temperatures decrease before increasing again in the Late Holocene. Both peat calibrations, MAT_{Naafs} and $MAT_{Crampton\text{-}Flood,}$ show more marked trends than the lake calibrations, $MAT_{Peterse}$ and MST_{Foster}. Highest temperature values are not reconstructed by the summer calibrations, but by the mean annual temperatures above zero calibration from Crampton-Flood *et al.* (2020). The GDGT-based temperature values are higher than the current values, and differ from those of pollen transfer-functions: we will therefore discuss trends rather than absolute values.

The warmest Holocene temperature appears to be at 4000 cal. yr BP, just before a temperature drop that spans the next 2000 years. This corresponds to the end of the HTM time frame reconstructed by the pollen transfer functions. However, it should be noted that from 6500 to 4000 cal. yr BP and from 1870 to 1330 cal yr BP and at 400 cal. yr BP, there is no interpretation of the calibration results, these samples having been excluded because of suspected correspondence to another community of brGDGTs. BrGDGTs analyzed in this study came from a peat sediment core, which adds temperature reconstruction biases (Weijers et al., 2010). It is more noteably more difficult to set up reconstructions of peatland or soil temperatures, because the modern data are less well known and/or less available, and also generally less used in paleoecology (Weijers et al., 2011, 2007b). The dual origin (terrestrial and lacustrine) of brGDGTs blurs the signal between the composition of brGDGTs and the calculation of CBT and therefore contributes to the error that accompanies them (Sun et al., 2011). Other biases in the reconstruction of temperatures from brGDGTs have been brought to light. The literature shows that brGDGT temperature calibrations are likely to both underestimate past temperatures (Li et al., 2017; Pearson et al., 2011; Tyler et al., 2010; Zink et al., 2010) but and at other times to overestimate them (Wang et al., 2012; Li et al., 2017), and this even with regional calibrations. The temperature seasonality, which is high in the region of the

study site, is a factor that enhances the overestimation of temperatures (Dearing Crampton-Flood et al., 2020) and this is what is clearly observed with all the calibrations that have been tested, compared to the modern average annual temperatures at Yaksha. Although bacterial communities are present and active in winter (Drotz et al., 2010; Nedwell, 1999), bacterial activity appears to be more intense in summer, with different bacterial communities than in the winter season (Schostag et al., 2015; Sun et al., 2011). The calibrations provided for high latitudes such as that of Foster *et al.* (2016), but also that of Dearing Crampton-Flood *et al.* (2020), more recently, with the use of their BayMBT0 model, would therefore correspond more to growing season, rather than to the mean annual temperature. External factors can also influence brGDGT distributions and temperature reconstructions, such as precipitation and humidity changes (Dearing Crampton-Flood et al., 2020). Finally, vegetation can also be an element of variability in the brGDGT production (from soils and from the watershed) (Ayari et al., 2013; Huguet et al., 2013; Naeher et al., 2014; Weijers et al., 2011). At Yaksha, the time periods that show the highest variability in the brGDGT signal are between 9100 and 8500 cal. yr BP, 5600 and 4700 cal. yr BP and 1500 cal. yr BP to the present day (Fig. 3C, CBT and IIIa/IIa indices, tetramethylated brGDGTs, rings tetra- and pentamethylated 5 Me brGDGTs). The alternation of light taiga and dark taiga could therefore have played a role in the diversity of the brGDGT present. This role is however not fully assessed so far (Buckles et al., 2014; Davtian et al., 2016; Weijers et al., 2010).

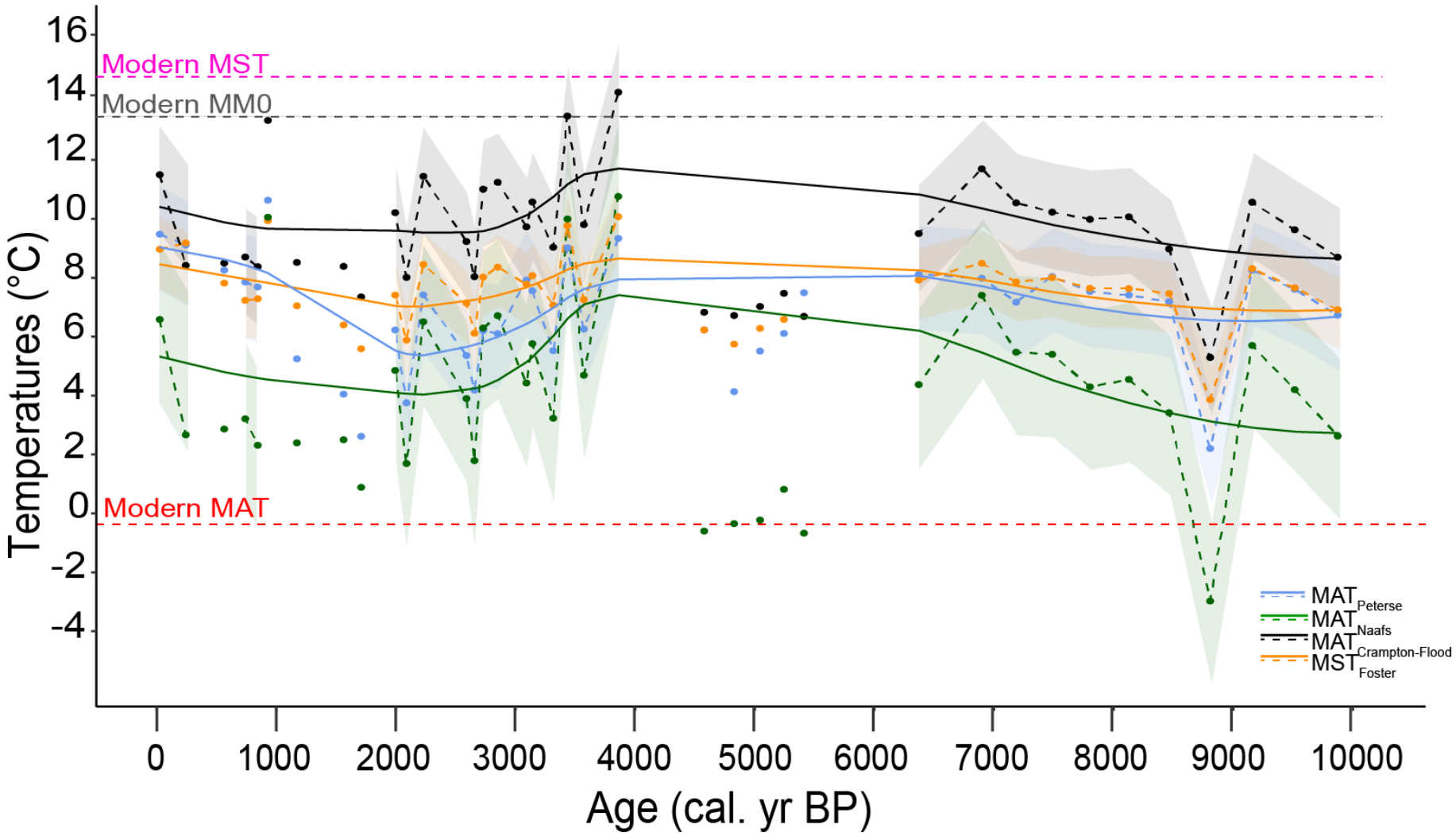

Figure 4: Yaksha GDGT temperature reconstructions. Blue: Mean Annual Temperature ($MAT_{Peterse}$) after Peterse et al. *(2012), green: Mean Annual Air Temperature (MAT_{Naafs}), after Naafs* et al. *(2017), black: Mean Annual Temperature above 0 ($MAT_{Crampton\text{-}Flood}$), after Dearing Crampton-Flood* et al. *(2020), orange: Mean Sub-Arctic Air Temperature (MST_{Foster}) after Foster* et al. *(2016). The reconstructed temperatures are smoothed with the R function Loess (span = 0.3). Modern Mean Annual Temperature (Modern MAT) is represented in red dotted line, Modern Mean Summer Temperature (Modern MST) is represented in pink dotted line and Modern Mean Months above 0°C Temperature (Modern MM0) is represented in grey dotted line.*

4.1.3 Pollen-inferred climate reconstructions

The reconstructed climatic parameters of the Holocene in the Republic of Komi show similar trends in the two-methods: MAT and WA-PLS (Fig. 2). A comparable agreement between the climate reconstructions obtained with the two methods can be observed at a more regional scale, namely the comparison between Europe and the Northern Hemisphere (Herzschuh et al., 2021). Here, the results from the MAT generally indicate more variability than the WA-PLS method, as has already been observed in other studies, because of the degree of sensivity of the method (Birks

and Seppä, 2004; Brewer et al., 2008; Dugerdil et al., 2021; Robles et al., 2022). The MAT has been widely used to reconstruct the climate changes in Europe over the Late Glacial and Holocene (Peyron et al., 2005, 2011, 2013; Mauri et al., 2015; Ponel et al., 2022) as the MAT is usually more sensitive to minor variations in the pollen assemblage, compared to the WA-PLS (Brewer et al., 2008; Sinopoli et al., 2019, Hershuzh et al., 2022). However, the MAT may be less reliable when the vegetation is only dominated by two or three taxa, as is the case in our study (Salonen et al., 2012). This is the reason the WA-PLS has been more often used than the MAT to reconstruct Holocene temperatures in the boreal regions of Scandinavia (Seppä et al., 2009; Salonen et al., 2011, 2012). The WA-PLS method is generally less efficient when the modern pollen dataset is large (Chevalier et al., 2020; Dugerdil et al., 2021), but in this study the dataset was reduced to records comparable in terms of biomes, which is also recommended as a method to increase the sensitivity of the MAT (Birks and Seppä, 2004). Moreover, the main disadvantage of WA-PLS is that it tends to overestimate values (Birks, 1998), which is observed in the results of our study. Our results show that in the Republic of Komi, the margins of error from the MAT (RSEP = 3.1 for TANN ; RSEP = 197.6 for PANN) are lower than those from the WA-PLS (RSEP = 4.3 for TANN ; RSEP = 266.7 for PANN). However, both methods appear fairly reliable because they provide similar trends for the Holocene.

4.1.4 Comparison of brGDGT- and pollen-inferred temperature reconstructions

The reconstructions based on brGDGTs and pollen show different absolute values and amplitudes of variations (Fig. 5A, B). With the brGDGT calibration of the temperatures, the amplitude of temperature variation is more than 7°C. In contrast with pollen records, the amplitude is around 4°C. However, the Holocene temperature variations comparing the two methods show more similarity. The Early Holocene begins with a slight drop in pollen-inferred temperatures, till about 8000 cal. yr BP, from which time the temperature trends rise. This corresponds fairly well with the brGDGT calibration $MAT_{Crampton\text{-}Flood}$, which shows an increase in temperatures during whole Early Holocene. The warmest period from pollen-inferred temperatures is recorded between 6800 and 4000 cal. yr. BP. At 4000 cal. yr. BP., the $MAT_{Crampton\text{-}Flood}$ calibration also shows its highest temperature, thus presenting a shared identification of the HTM between the two temperature reconstruction methods (the mid-Holocene part of the brGDGT temperature calibrations being put to one side and not compared with pollen-inferred temperatures). Thereafter, trends for both signals are similar, since a synchronous decrease in temperatures is indicated after 4000 cal. yr BP, followed by a net increase from 3000 cal. yr BP for the pollen signal and from 2000 cal. yr BP for the brGDGT calibration.

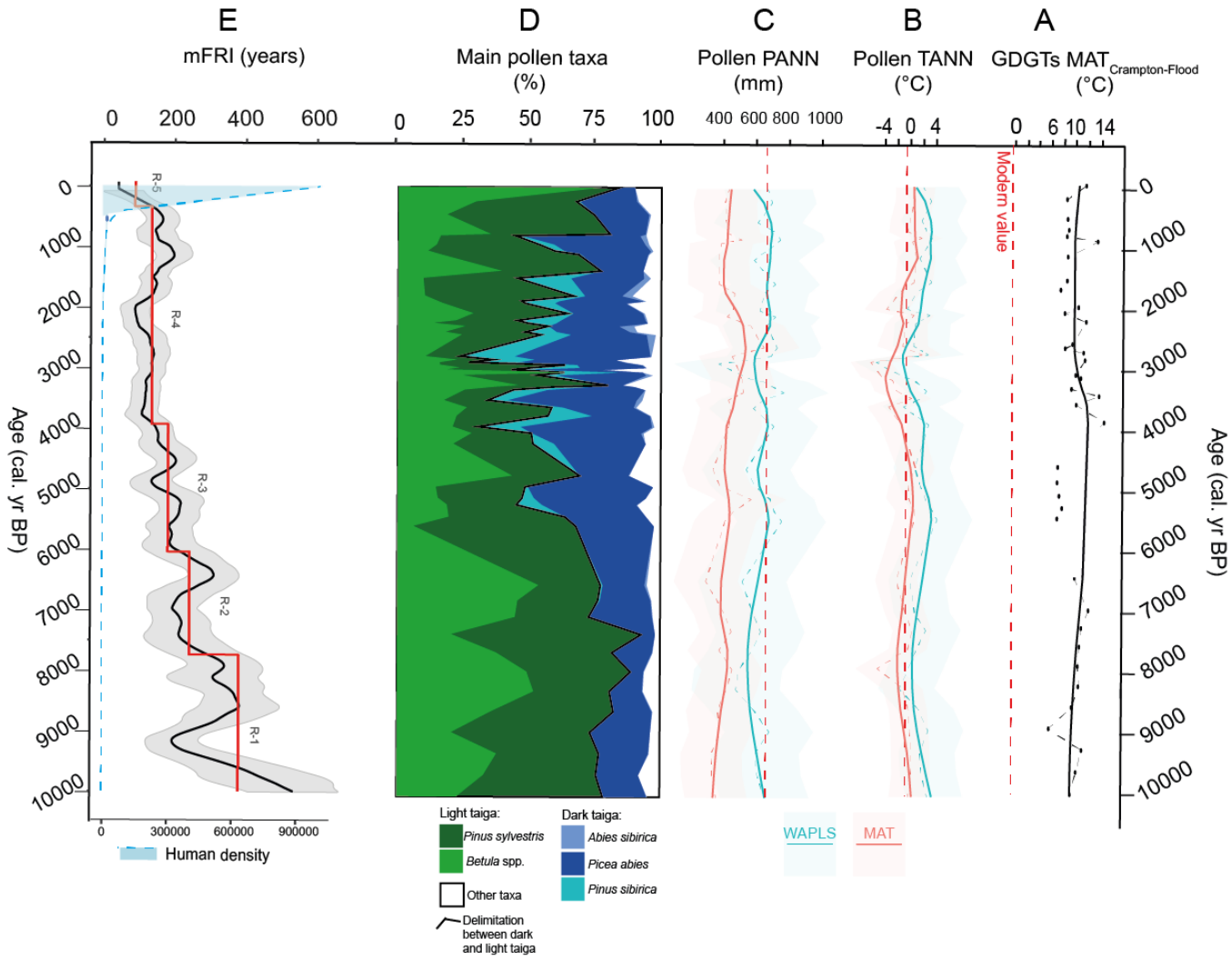
E
mFRI (years)
0 200 400 600
D
Main pollen taxa (%)
0 25 50 75 100
C
Pollen PANN (mm)
400 600 800 1000
B
Pollen TANN (°C)
-4 0 4
A
GDGTs MAT Crampton-Flood (°C)
0 6 10 14
Modern value
Age (cal. yr BP)
0 1000 2000 3000 4000 5000 6000 7000 8000 9000 10000
R-5
R-4
R-3
R-2
R-1
0 300000 600000 900000
Human density
Light taiga:
Pinus sylvestris
Betula spp.
Other taxa
Delimitation between dark and light taiga
Dark taiga:
Abies sibirica
Picea abies
Pinus sibirica
WAPLS
MAT

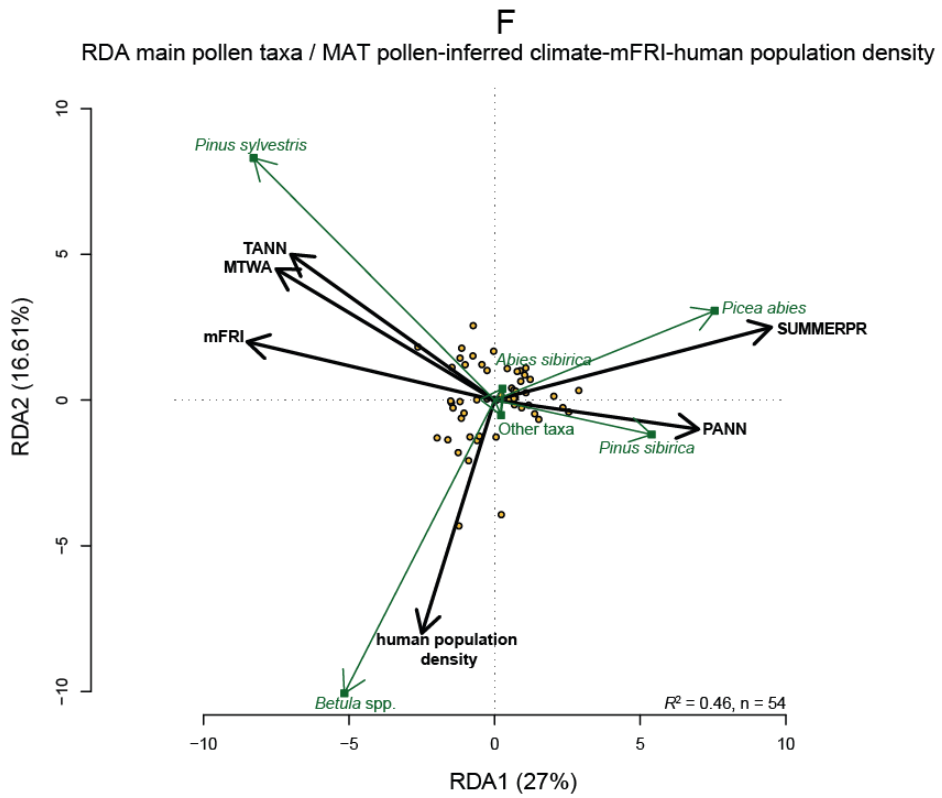
F
RDA main pollen taxa / MAT pollen-inferred climate-mFRI-human population density
RDA2 (16.61%)
10 5 0 −5 −10
Pinus sylvestris
TANN
MTWA
mFRI
Picea abies
SUMMERPR
Abies sibirica
Other taxa
PANN
Pinus sibirica
human population density
Betula spp.
R² = 0.46, n = 54
−10 −5 0 5 10
RDA1 (27%)

Figure 5: Yaksha local dynamics. A: brGDGT-inferred temperatures $MAT_{Crampton\text{-}Flood}$, after Dearing Crampton-Flood et al. *(2020). B: Pollen-inferred mean annual temperatures TANN. C: Pollen-inferred mean annual precipitation MAP. D: Main pollen taxa cumulative diagram. E: Mean Fire Return Interval and human population density in the Republic of Komi (mFRI, Barhoumi* et al.*, 2019, 2020). F: RDA for Yaksha main pollen taxa, MAT reconstructed climate (TANN, PANN, MTWA, SUMMERPR); fire activity (mFRI) and human activity (human population density).*

4.2 Yaksha local dynamics: interactions between climate, vegetation, fire and human presence

4.2.1 From 10,000 to 4000 cal. yr BP: a first half of the Holocene mainly influenced by climate

To evaluate the background for fire dynamics, a Pearson correlation test was carried out between modern annual temperatures (from 2010 to 2018), for the studied sites, and the mean temperatures of the warmest months, (June, July, August) , corresponding to the fire season, as well as correlation with mean temperatures of the months above 0°C (Tabatabai et al., 2021). The Pearson's correlation indicates that modern mean annual temperatures are positively correlated with mean modern summer temperatures (correlation of 0.45) and mean modern temperatures of months above 0°C (correlation of 0.48). It is therefore assumed that past annual mean temperatures, reconstructed from pollen and brGDGTs were also positively correlated with past mean summer temperatures and past mean temperatures of months above 0°C.

Temperatures close to the modern ones are reconstructed from 10,000 to 9000 cal. yr BP (Fig. 5B) with vegetation mainly representative of the light taiga type, with the taxa *Pinus sylvestris* and *Betula* spp. being dominant (75 %, Fig. 5D). These results are consistent with those for the modern period.

Even though the light taiga remained in the main forest system up to 5500 cal. yr BP, the warming occurring since 8000 and including the HTM, which lasted until 4000 cal. yr BP, is associated with an increase of dark taiga taxa (increase in *Picea abies* and appearance of *Pinus sibirica*). These two taxa seem to be influenced by the increase in the mean annual and summer precipitation, as shown by the RDA (Fig. 5F), which occurs at the same time. The increase in dark taiga taxa is consistent with the recognised characteristics of this taiga system, which is favored by precipitation (Goldammer and Furyaev, 1996; Golubeva, 2008; Schulze et al., 2005). The increase could also demonstrate the substantial influence of climate on vegetation dynamics during this period. Moreover, between 10,000 and 6000 cal. yr BP, the mean Fire Return Interval (mFRI) based on charcoal analysis (Barhoumi et al., 2019) is high (median mFRI greater than 200 years, Fig. 5E), which would be indicative of a boreal forest with larger occurrence of the dark taiga type in the earlier part of the Holocene, because the dark taiga is usually associated with low fire frequency (de Groot et al., 2013; Goldammer and Furyaev, 1996; Sannikov and Goldammer, 1996). Since the human presence and its impact on

397 the environment is negligible in the first half of the Holocene (between 10,000 and 5000 cal. yr BP; Drobyshev *et al.*, 2004; Karmanov *et al.*,
398 2011; Klein Goldewijk *et al.*, 2011), the climate appears to have been the main factor influencing the vegetation in Yaksha. This is consistent
399 with the conclusions of a previous study based on pollen analysis and vegetation cover modeled by REVEALS, over the period from 10,000 to
400 6000 cal. yr BP (Barhoumi *et al.* (2020).

401

402 ### *4.2.2 From 4000 to 600: an increasing impact of fires*

403 The period between 4000 and 2500 cal. yr BP corresponds to a significant decrease in temperature (Fig. 5A, B). The percentage ratio between
404 dark taiga and light taiga shows great variability and seems to demonstrate the establishment of a boreal forest consisting of dark and light taiga
405 mosaic patches, equally distributed, supported by high precipitation favouring dark taiga. However, this period coincides with the crossing of a
406 threshold in the fire regime of Yaksha: the mFRI goes from 180 years (Fig 5E, phase R-3) to 135 years (phase R-4) from 4000 cal. yr BP up to
407 600 cal. yr BP. An mFRI value of *circa* 200 years corresponds to a fire frequency still tolerable by the representative taxa of the dark taiga
408 (Goldammer and Furyaev, 1996; Sannikov and Goldammer, 1996). But from 4000 cal. yr BP, the mFRI value is well below this threshold and
409 should no longer allow dark taiga to develop (Goldammer and Furyaev, 1996; Schulze et al., 2005). A higher fire frequency would benefit the
410 maintenance of a light taiga system, while high precipitation would maintain the presence of dark taiga taxa such as *Picea abies*. The contrasting
411 influences of the climate and the fire regimes could explain the maintenance of a forest composed of a mosaic of patches of dark and light taiga
412 The gradual return to a light taiga dominance between 2500 and 600 cal. yr BP therefore seems favored by the increase of temperatures, but also
413 by the establishment of the lower mFRI, since this type of forest is made up of fire-tolerant species well adapted to high fire frequency (see RDA,
414 *Pinus sylvestris* correlated with mean temperatures and mFRI), (Goldammer and Furyaev, 1996; Schulze et al., 2005). Fire frequency could be
415 the cause of the decline of *Abies sibirica* and *Pinus sibirica*, which are not resistant to frequent fire events and whose seed production and life
416 cycle may need a longer time than the time interval available between two fire events during this phase (Goldammer and Furyaev, 1996; Sannikov
417 and Goldammer, 1996; Schulze et al., 2005). The dominant presence of light taiga over dark taiga from 2500 cal. yr BP, does not prevent *Picea*
418 *abies* remaining well established. Barhoumi *et al.*, (2020) suggested that this may be due to the local establishment of *Picea abies* tree stands,
419 growing along small streams and moist soils and with precipitation staying high between 3000 and 2000 cal. yr BP (Zaretskaya et al., 2014). As
420 these systems are also present in light taiga, it is surprising to note that *Picea abies* does not suffer drastically from the drop in mFRI to below
421 200 years. In theory, *Picea abies* cannot develop if surface fires reach its critical regeneration time range (about 200 years after a fire event)

(Goldammer and Furyaev, 1996; Schulze et al., 2005). We therefore suggest that these surface fires were not able to reach the peat wetlands on which *Picea abies* grew. That interpretation was highlighted by the first study on the dynamics of fires of the Yaksha site by Barhoumi *et al.* (2019). This study highlights that most of the recent fires revealed by the analysis of fire scars on trees at the Yaksha site, have affected the vegetation in a very localized way, while others have affected the site Yaksha as a whole. This demonstrates that the surface fires at the Yaksha site could have been mostly local, and so were not able to reach the populations of *Picea abies*, because of their location on highly moist soils.

4.2.3 From 600 to modern times: the combined influence of human activity and climate?

The period between 600 and 0 cal. yr BP shows slightly increasing temperature values to levels similar to those of the Early Holocene, and stable precipitation (Fig. 5A). The light taiga is well established and *Betula spp.* is dominant (Fig. 5D). *Betula* is a pioneer species in a disturbed environment and is also a sign of the opening of the boreal forest in this zone (Goldammer and Furyaev, 1996). The strong presence of *Betula spp.* during this phase is strongly associated with human population density in the RDA (Fig. 5F) and could be a sign of a human influence on the vegetation. In the Republic of Komi in particular, logging is now a highly developed activity and its production represents a major economic resource for this region (Naryshkin, 2003). The mFRI is at its lowest value within the Holocene interval (less than 100 years, phase R-5, Fig. 5E). This time frame corresponds to the highest density of the human population in the Republic of Komi and its increasing activity and impact on its environment (Drobyshev et al., 2004b; Klein Goldewijk et al., 2011; Naryshkin, 2003). It therefore seems that fire events could have been induced by human activity and that the generally high fire activity of this period could be related to both anthropogenic influences and a more favorable climate (Drobyshev et al., 2004b; Naryshkin, 2003). However, a recent study has nuanced the impact of human presence during this period. Different waves of human colonization during this period were indeed indicated, but were not synchronous with the changes in the fire cycles reconstructed by dendrochronological analyses (Ryzhkova et al., 2022). These authors deduced that the climate was the main factor in the dynamics of the forest and that the human impact on fire activity was more pronounced after the 1900s. This is also consistent with the increase in temperature reconstructed by brGDGTs, which started from 1800 cal. yr BP but intensified from about 700 cal. yr BP (Fig. 5A).

4.3 Regional climate pattern in the South of the Republic of Komi

4.3.1 From 10,000 to 8000 cal. yr BP, a cold Early Holocene

Although AO/NAO dynamics influence the climate of Republic of Komi region *(Raspopov et al., 2013)*, climate records from the region can be different from those recorded, for example, in Siberia because the Republic of Komi is located in a boundary zone, at the limit between the regions positively or negatively influenced by atmospheric processes and solar irradiation *(Raspopov et al., 2013)*. The regional climate signal in the South of the Republic of Komi indicates a cooling and drying in the Early Holocene (Fig. 6H, 6I and 8A). This is in agreement with (1) the brGDGT temperature calibration being the coldest of the records at the Yaksha site (Fig. 6J), (2) reconstructions of mean annual temperatures in Eastern-central European Russia (from +1 to -1°C, Fig. 6E, Novenko and Olchev, 2015),summer temperatures in Eastern Siberia inferred from chironomids (from +17 to +14°C, Fig. 6G, Nazarova *et al.*, 2015), (3) climate model simulations and mean temperature anomalies of Europe, inferred from pollen (WA-PLS), showing the lowest temperatures of the Holocene during this time (between -1 to 0°C anomaly for annual temperatures, Fig. 6B, C, Herzschuh et al., 2022) The GCM outputs also simulate a drop in summer temperatures for Central Asia with a loss of about 0.5°C, Fig. 6M, (Bush, 2005). However, in North Eastern European Russia, a rise in summer temperatures is reconstructed from pollen data (+1°C approximately, Fig. 6D, Salonen *et al.*, 2011). The South of the Republic of Komi, therefore, seems to have undergone climatic influences similar to those occurring in Western Russia and in Siberia.

459

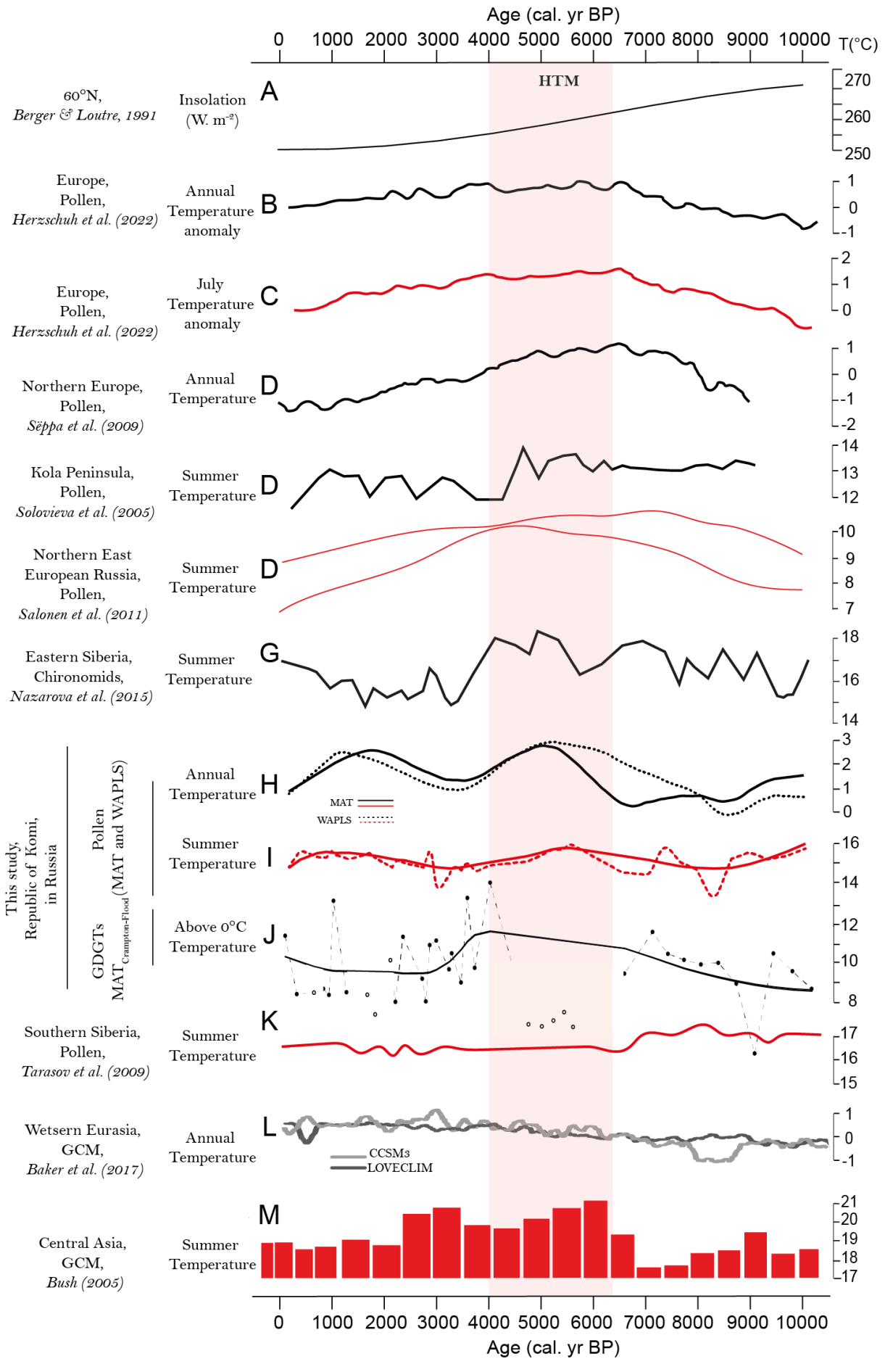
Age (cal. yr BP)
0 1000 2000 3000 4000 5000 6000 7000 8000 9000 10000
T(°C)
HTM
60°N, Berger & Loutre, 1991
Insolation (W. m⁻²)
A
270 260 250
Europe, Pollen, Herzschuh et al. (2022)
Annual Temperature anomaly
B
1 0 -1
Europe, Pollen, Herzschuh et al. (2022)
July Temperature anomaly
C
2 1 0
Northern Europe, Pollen, Sëppa et al. (2009)
Annual Temperature
D
1 0 -1 -2
Kola Peninsula, Pollen, Solovieva et al. (2005)
Summer Temperature
D
14 13 12
Northern East European Russia, Pollen, Salonen et al. (2011)
Summer Temperature
D
10 9 8 7
Eastern Siberia, Chironomids, Nazarova et al. (2015)
Summer Temperature
G
18 16 14
This study, Republic of Komi, in Russia
Pollen (MAT and WAPLS)
GDGTs MAT Crampton-Flood
Annual Temperature
H
MAT
WAPLS
3 2 1 0
Summer Temperature
I
16 14 12 10 8
Above 0°C Temperature
J
Southern Siberia, Pollen, Tarasov et al. (2009)
Summer Temperature
K
17 16 15
Wetsern Eurasia, GCM, Baker et al. (2017)
Annual Temperature
L
CCSM3
LOVECLIM
1 0 -1
Central Asia, GCM, Bush (2005)
Summer Temperature
M
21 20 19 18 17
0 1000 2000 3000 4000 5000 6000 7000 8000 9000 10000
Age (cal. yr BP)

Figure 6: Synthesis of Holocene temperature reconstructions in the Republic of Komi and neighboring regions, based on pollen, GDGTs, chironomids and GCM outputs. Mean annual and summer temperatures are represented in black and in red, respectively. Location of the sites are represented in Fig. 1. Insolation at 60°N after Berger and Loutre (1991). The red rectangle indicates the HTM period.

4.3.2 Timing of the HTM

In the Republic of Komi, pollen results suggest the occurrence of the HTM between 6800 and 4000 cal. yr BP (this time frame includes the high mean annual temperature values for both MAT and WA-PLS methods, Fig. 6H). This finding is consistent with the brGDGT $MAT_{Crampton\text{-}Flood}$ calibration, recording its warmest temperature value at 4000 cal. yr BP (Fig. 6J). The increase in annual temperatures in the Republic of Komi is also associated with an increase in precipitation (Fig. 7B). This HTM time window is consistent with but broader than the one suggested by Golubeva (2008), with the same pollen data set (except Yaksha site) but using other methods of temperature reconstruction (Klimanov, 1976). This time-range for the HTM reconstructed with MAT/WA-PLS techniques is consistent with that reconstructed by Herzschuh *et al.* (2022), showing a pollen-inferred (WA-PLS method) HTM at 5600 cal. yr BP for Europe annual temperatures. This time range is also consistent with the Russian Arctic region and Kola Peninsula pollen-based temperature reconstructions (Fig. 6K; Tarasov *et al.*, 1999; Andreev and Klimanov, 2000; Solovieva, Tarasov and MacDonald, 2005), in the North of the Republic of Komi. The Russian Arctic HTM was explained because the Arctic Ocean coast was about 100 to 300 km further North at this time than it is today, which contributed to a warmer and more continental climate (Andreev and Klimanov, 2000; Baranskaya et al., 2018). Studies from the west of the Republic of Komi, in Siberia and in Central Yakutia also show an climatic optimum included in this interval (Biskaborn et al., 2016; Blyakharchuk and Sulerzhitsky, 1999; Nazarova et al., 2015b; Subetto et al., 2017; Ulrich et al., 2017). Moreover, from 10,000 cal. yr BP until 4000 cal. yr BP, climate was the most moist of the Holocene (Blyakharchuk and Sulerzhitsky, 1999; Tarasov et al., 2009, 1999), which partially corresponds with the precipitation records from the Republic of Komi (since it was low between 10,000 and 8500 cal. yr BP, and high between 6500 and 4000 cal. yr BP). The climate became moist again between 3000 and 600 cal. yr BP. This time frame corresponds well with the annual precipitation reconstruction from Herzschuh et al. (2022), suggesting that the Holocene rincrease in precipitation could be due to enhanced cyclonic activity. The HTM in the Republic of Komi is not as long as in Northern Europe and Fennoscandia, where it began as early as 8000 cal. yr BP (Fig. 6B and 7D; Seppä *et al.*, 2009; Salonen *et al.*, 2011). Another extended HTM was observed by Kultti *et al.* (2003), still closer to Republic of Komi, between 9000 to 5200 cal. yr BP. Some of the sites in the Kultti study were located at high altitudes in the Urals. The altitude may have had an impact on the different climatic influences affecting the area from Arctic Russia to the Vychegda river basin in Republic of Komi. Many studies highlight the role of increased insolation in global warming during the HTM (Bartlein et al., 2011; Kultti et al., 2003; Mayewski et al., 2004; Wohlfarth et al., 2007).

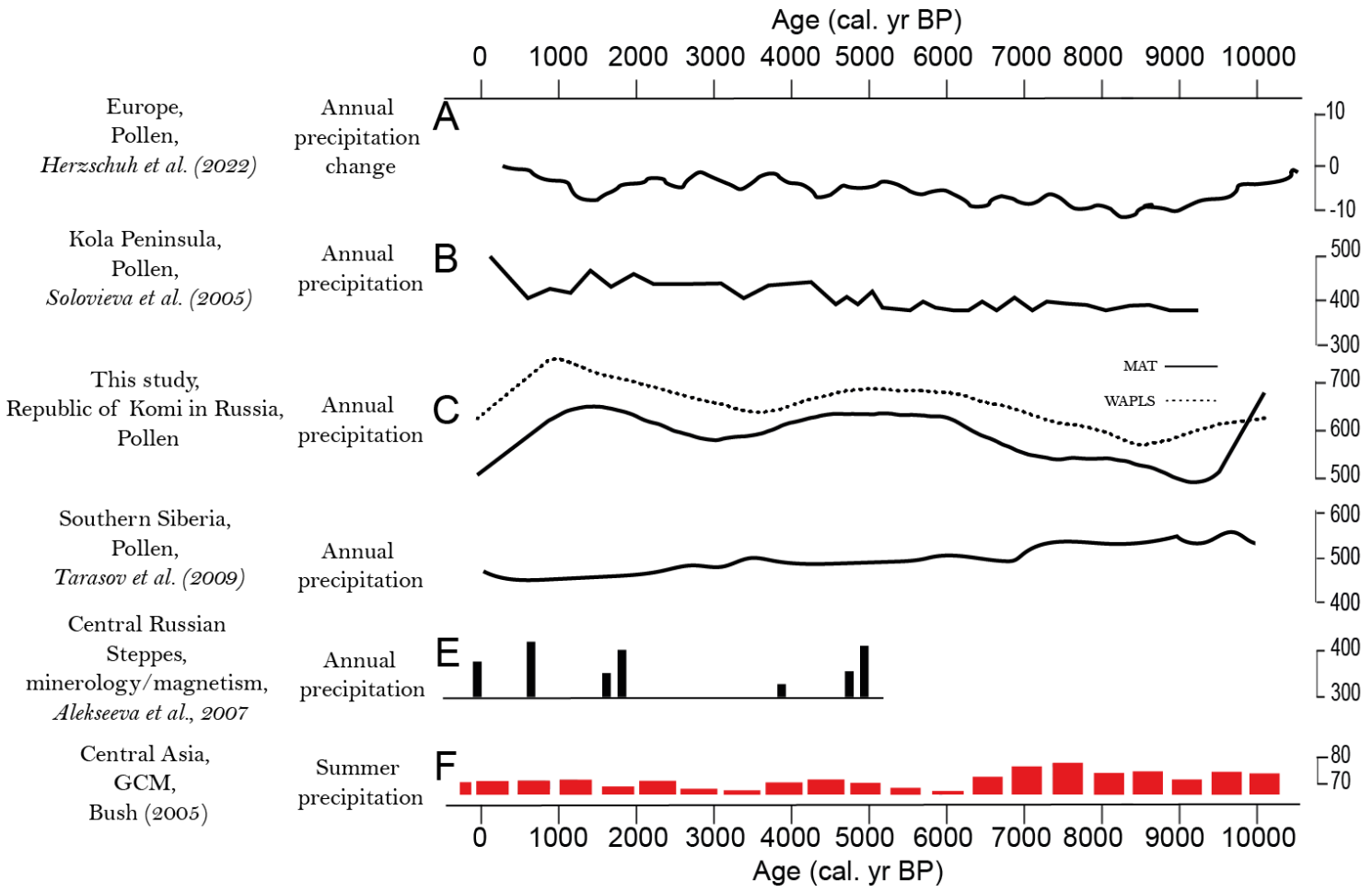

Figure 7: Synthesis of Holocene precipitation reconstructions in the Republic of Komi and neighboring regions, based on pollen, minerology/magnetism and GCM outputs. Annual sum of precipitation is represented in black and the summer sum of temperatures, in red. Location of the sites are represented in Fig. 1

Atmospheric processes could also explain this HTM period: a strong Westerly circulation, with a strong AO/NAO positive phase in winter (which would have generated warm and moist climates in Northern Europe) and a weaker AO/NAO positive phase in summer (warm and dry climate) (Mauri et al., 2015). Salonen *et al.* (2011) have also discussed the observed lags in HTM from Fennoscandia to the Ural region. Their assumptions are (1) there is a geographical timing gradient of the HTM; (2) some reconstructions may be wrong due to biases in the temperature inference methods used; (3) the different proxies for calculating temperatures may have non-synchronous responses to warming and (4) the complex history of tree lines in Russia may add uncertainties regarding pollen-based reconstructions.

4.3.3 Late Holocene, from 4000 to modern time: cold phase, MWP and LIA?

A fluctuating and colder phase is marked in the Republic of Komi between 4000 and 2500 cal. yr BP. This cooling seems to have been also registered in Siberia by chironomids (summer temperatures) (Nazarova et al., 2015b) and in Arctic Russia (Andreev and Klimanov, 2000). In Northern Europe, a large period of continuous and gradual cooling has extended since the end of the HTM, around 4000 cal. yr BP, up to 1000 cal. yr BP, and has been largely explained by the influence of the decrease in summer insolation (Fig. 6D; Salonen *et al.*, 2011).

According to Seppä *et al.*, (2009), the Medieval Warm Period (MWP, 1550-650 cal. yr BP (Camill et al., 2009)) is not a distinct temperature peak in Northern Europe, but "represents the final centuries of a longer warm period before the onset of cooling". Pollen signals from the Republic of Komi clearly indicate a period of warming between 2000 and 900 cal. yr BP. This signal is also registered by pollen assemblages from the Kola Peninsula, which is located in the Northern part of European Russia (Solovieva et al., 2005) and a general slight increase in summer temperatures has been simulated for Central Asia (Bush, 2005). This period coincides with the wettest recorded in the Republic of Komi, the Kola Peninsula and the Central steppes of Russia, based on pollen grains and magnetism/minerological analysis (Fig. 7B, A and E; Solovieva, Tarasov and MacDonald, 2005; Alekseeva *et al.*, 2007).

The subsequent short and rapid decrease in temperatures in the Republic of Komi from 500 cal. yr BP (WA-PLS), may correspond to the Little Ice Age (LIA, 650-150 cal. yr BP (Camill et al., 2009)) . This cooling was also noted in records from Northern Europe by Seppä *et al.* (2009) until ca. 400 cal. yr BP, in West-central Eurasia by the LOVECLIM model (Baker *et al.*, 2017), in Northern East European Russia by Salonen *et al.* (2011), and in the Kola Peninsula (Solovieva et al., 2005). However, the resolution of our records is too low to corroborate (or to refute) these results, but there are consistent with these observations.

At the end of the 19th century, a global warming trend was recorded by tree-rings in the Northern Urals (Moiseev et al., 2010) (Moiseev *et al.*, 2010) but in the Republic of Komi, the results do not show any general warming trend during this period, except for the sites Yaksha (MAT) and Kalya. The brGDGT calibrations also showed also an increase in temperature over this interval.

5. Conclusions and remarks on the Republic of Komi boreal forest

This study presents (1) the first Holocene temperature reconstruction at a regional scale of the southern part of the Republic of Komi, based on the study of pollen- transfer functions based on six different sites. (2) the first study of the local dynamics in Yaksha, between climate (based on pollen-transfer functions and brGDGT temperature calibrations), fire, vegetation and human activities.

Regional climate reconstructions for the Republic of Komi show an increase in precipitation and a mid-Holocene HTM between 6800 and 4000 cal. yr BP which is in line with neighboring regions in Northern Europe, and also with Siberia, through the analysis of different proxies and analytical methods (pollen, chironomids, model outputs).

At the local scale of Yaksha, the temperature reconstructions based on pollen assemblages and brGDGTs show common warmest temperature phases around 4000 cal. yr BP. Further studies of cold environments are needed to improve the calibrations for brGDGTs, in particular for the Holocene, where factors others than temperature influence the composition of brGDGT communities.

Finally, our study showed that climate had a major influence on the vegetation and dynamics of the boreal forest in Yaksha. Fires had an additional and growing impact on vegetation dynamics between 4000 and 600 cal. yr BP. Finally, from 600 BP to the present day, both climate and increasing human impacts have influenced the dynamics of the boreal forest in this region. In modern times, the fire regime induced by anthropogenic activities corresponds to an overexploitation of the forest, whose coniferous species have rapidly declined in favor of a pioneer deciduous species (the explosion of *Betula spp.* from 600 to the modern age is demonstates this effect (Naryshkin, 2003; Sannikov and Goldammer, 1996). It is likely that the wetter dark taiga growing on organic soils has been weakened by this fire regime. This can then lead to a reversal of the balance in the carbon cycle, which could lead to massive releases into the atmosphere. This observation was made by Naryshkin, (2003) and Walker *et al.* (2019): not only do these forests no longer play the role of carbon sinks as they have done in the past, but they are gradually becoming sources of atmospheric carbon. With global warming, the temperature and dryness conditions of the environment may increase even more, and induce a greater dryness of the soil, allowing the spread of fires even on previously more moist areas and therefore affect tree populations which were not previously vulnerable. This was the case for example in the years 1972, 1974, 1977, 1982, 1987, 1998 in Siberia and in more recent years in Siberia and in the Ural region (Goldammer et al., 2005; Goldammer and Furyaev, 1996). Managing the structure of forest stands by establishing species more adapted to the new local climatic conditions may help to reverse the impact on the increase in fire activity that is evident today.

6. Acknowledgements

This study was funded by the Russian Fund for Basic Research (RFBR) under the project #20-04-00568 (to I.D.) and was supported by the Canadian National Research Council Canada through Discovery Grant (grant # DDG-2015-00026 to I.D.), the Swedish Research Council FORMAS (grant #239-2014-1866 to I.D.), the Swedish Institute funded networks CLIMECO, the BalticFire (#10066-2017-13 and #24474/2018 to I.D.), the Scientific and Educational Center “Russian Arctic: New Materials, Technologies and research Methods” (to A.K.), the Belmont Forum Project PREREAL (grant #292-2015-11-30-13-43-09 to I.D.) and the Ministry of Education of the Russian Federation (project #FSZN 2020-0016 to D.S.; #0185-2021-0018 to A.K.). The study was conducted within the framework of the NordicProxy network, which is supported by the Nordic Forest Research (SNS), the consortium GDRI Cold Forests and Institut Universitaire de France of Adam A. Ali. For the analytical work completed at LGLTPE- ENS de Lyon, this research was funded by Institut Universitaire de France funds to Guillemette Ménot. This is an ISEM contribution No... We would like to thank Nina Ryzhkova and the team of the Siberian Institute of Plant Physiology and Biochemistry, directed by Viktor Ivanovich Voronin in Irkutsk, for helping us with logistics during one of our fieldwork expeditions, related to the PhD project from which this paper is issued, and Sandrine Canal for her general contribution towards technical analysis of Yaksha samples. We would also like to thank Mary Robles for her general help with discussion of pollen transfer functions and brGDGT analysis.

7. Bibliography

Alekseeva, T., Alekseev, A., Maher, B.A., Demkin, V., 2007. Late Holocene climate reconstructions for the Russian steppe, based on mineralogical and magnetic properties of buried palaeosols. Palaeogeography, Palaeoclimatology, Palaeoecology 249, 103–127. https://doi.org/10.1016/j.palaeo.2007.01.006

Ali, A.A., Blarquez, O., Girardin, M.P., Hély, C., Tinquaut, F., El Guellab, A., Valsecchi, V., Terrier, A., Bremond, L., Genries, A., 2012. Control of the multimillennial wildfire size in boreal North America by spring climatic conditions. Proceedings of the National Academy of Sciences 109, 20966–20970.

Andreev, A., Klimanov, V., 2000. Quantitative Holocene climatic reconstruction from Arctic Russia. Journal of Paleolimnology 24, 81–91.

Andreev, A.A., Klimanov, V.A., n.d. Quantitative Holocene climatic reconstruction from Arctic Russia 12.

Andreev, A.A., Siegert, C., Klimanov, V.A., Derevyagin, A.Y., Shilova, G.N., Melles, M., 2002. Late Pleistocene and Holocene vegetation and climate on the Taymyr lowland, northern Siberia. Quaternary Research 57, 138–150.

Ayari, A., Yang, H., Wiesenberg, G.L., Xie, S., 2013. Distribution of archaeal and bacterial tetraether membrane lipids in rhizosphere-root systems in soils and their implication for paleoclimate assessment. Geochemical Journal 47, 337–347.

Baker, J.L., Lachniet, M.S., Chervyatsova, O., Asmerom, Y., Polyak, V.J., 2017. Holocene warming in western continental Eurasia driven by glacial retreat and greenhouse forcing. Nature Geosci 10, 430–435. https://doi.org/10.1038/ngeo2953

Baranskaya, A.V., Khan, N.S., Romanenko, F.A., Roy, K., Peltier, W.R., Horton, B.P., 2018. A postglacial relative sea-level database for the Russian Arctic coast. Quaternary Science Reviews 199, 188–205. https://doi.org/10.1016/j.quascirev.2018.07.033

Barhoumi, C., Ali, A.A., Peyron, O., Dugerdil, L., Borisova, O., Golubeva, Y., Subetto, D., Kryshen, A., Drobyshev, I., Ryzhkova, N., 2020. Did long-term fire control the coniferous boreal forest composition of the northern Ural region (Komi Republic, Russia)? Journal of Biogeography 47, 2426–2441.

Barhoumi, C., Peyron, O., Joannin, S., Subetto, D., Kryshen, A., Drobyshev, I., Girardin, M.P., Brossier, B., Paradis, L., Pastor, T., 2019. Gradually increasing forest fire activity during the Holocene in the northern Ural region (Komi Republic, Russia). The Holocene 0959683619865593.

Barhoumi, C., Vogel, M., Dugerdil, L., Limani, H., Joannin, S., Peyron, O., Ali, A.A., 2021. Holocene Fire Regime Changes in the Southern Lake Baikal Region Influenced by Climate-Vegetation-Anthropogenic Activity Interactions. Forests 12, 978. https://doi.org/10.3390/f12080978

Bartlein, P.J., Harrison, S., Brewer, S., Connor, S., Davis, B., Gajewski, K., Guiot, J., Harrison-Prentice, T., Henderson, A., Peyron, O., 2011. Pollen-based continental climate reconstructions at 6 and 21 ka: a global synthesis. Climate Dynamics 37, 775–802.

Berger, A., Loutre, M.-F., 1991. Insolation values for the climate of the last 10 million years. Quaternary Science Reviews 10, 297–317.

Bezrukova, E.V., Hildebrandt, S., Letunova, P.P., Ivanov, E.V., Orlova, L.A., Müller, S., Tarasov, P.E., 2013. Vegetation dynamics around Lake Baikal since the middle Holocene reconstructed from the pollen and botanical composition analyses of peat sediments: Implications for paleoclimatic and archeological research. Quaternary International 290–291, 35–45. https://doi.org/10.1016/j.quaint.2012.10.043

Bezrukova, E.V., Letunova, P.P., Vershinin, K.E., Krivonogov Sergey, K., Abzaeva, A.A. (Abzayeva, Krapivina, S.M., Khomutova, M.Y., 2003. Paleoenvironmental changes in Baikal Basin in the late glacial and Holocene. Berliner Palaeobiologische Abhandlungen 4, 111–120.

Birks, H., 1998. DG Frey and ES Deevey Review 1: Numerical tools in palaeolimnology–Progress, potentialities, and problems. Journal of paleolimnology 20, 307–332.

Birks, H.J.B., Seppä, H., 2004. Pollen-based reconstructions of late-Quaternary climate in Europe–progress, problems, and pitfalls. Acta Palaeobotanica 44, 317–334.

Biskaborn, B.K., Subetto, D.A., Savelieva, L.A., Vakhrameeva, P.S., Hansche, A., Herzschuh, U., Klemm, J., Heinecke, L., Pestryakova, L.A., Meyer, H., Kuhn, G., Diekmann, B., 2016. Late Quaternary vegetation and lake system dynamics in north-eastern Siberia: Implications for seasonal climate variability. Quaternary Science Reviews, Special Issue: PAST Gateways (Palaeo-Arctic Spatial and Temporal Gateways) 147, 406–421. https://doi.org/10.1016/j.quascirev.2015.08.014

Blyakharchuk, T.A., Sulerzhitsky, L.D., 1999. Holocene vegetational and climatic changes in the forest zone of Western Siberia according to pollen records from the extrazonal palsa bog Bugristoye. The Holocene 9, 621–628. https://doi.org/10.1191/095968399676614561

Borisova, O.K., 2002. The Holocene flora and vegetation of the northern Russian Plain (the Vychegda River basin). Acta Palaeontologica Sinica 41, 478–486.

606 Brewer, S., Guiot, J., Sánchez-Goñi, M., Klotz, S., 2008. The climate in Europe during the Eemian: a multi-method approach using pollen data.
607 Quaternary Science Reviews 27, 2303–2315.
608 Buckles, L., Weijers, J., Tran, X.-M., Waldron, S., Sinninghe Damsté, J., 2014. Provenance of tetraether membrane lipids in a large temperate
609 lake (Loch Lomond, UK): implications for glycerol dialkyl glycerol tetraether (GDGT)-based palaeothermometry. Biogeosciences 11,
610 5539–5563.
611 Bush, A.B.G., 2005. CO2/H2O and orbitally driven climate variability over central Asia through the Holocene. Quaternary International,
612 Paleolimnological records from Asian lacustrine systems: archives of large scale seasonal atmospheric circulation changes in the
613 northern hemisphere 136, 15–23. https://doi.org/10.1016/j.quaint.2004.11.004
614 Camill, P., Barry, A., Williams, E., Andreassi, C., Limmer, J., Solick, D., 2009. Climate-vegetation-fire interactions and their impact on long-
615 term carbon dynamics in a boreal peatland landscape in northern Manitoba, Canada. Journal of Geophysical Research: Biogeosciences
616 114.
617 Cao, J., Rao, Z., Jia, G., Xu, Q., Chen, F., 2017. A 15 ka pH record from an alpine lake in north China derived from the cyclization ratio index
618 of aquatic brGDGTs and its paleoclimatic significance. Organic Geochemistry 109, 31–46.
619 Cheung, H., Zhou, W., 2015. Implications of Ural blocking for East Asian winter climate in CMIP5 GCMs. Part II: Projection and uncertainty
620 in future climate conditions. Journal of Climate 28, 2217–2233.
621 Cheung, H.H., Zhou, W., 2015. Implications of Ural blocking for east Asian winter climate in CMIP5 GCMs. Part I: biases in the historical
622 scenario. Journal of Climate 28, 2203–2216.
623 Cheung, H.N., Zhou, W., Mok, H.Y., Wu, M.C., 2012. Relationship between Ural–Siberian blocking and the East Asian winter monsoon in
624 relation to the Arctic Oscillation and the El Niño–Southern Oscillation. Journal of Climate 25, 4242–4257.
625 Cheung, H.N., Zhou, W., Shao, Y., Chen, W., Mok, H.Y., Wu, M.C., 2013. Observational climatology and characteristics of wintertime
626 atmospheric blocking over Ural–Siberia. Climate dynamics 41, 63–79.
627 Chevalier, M., Davis, B.A., Heiri, O., Seppä, H., Chase, B.M., Gajewski, K., Lacourse, T., Telford, R.J., Finsinger, W., Guiot, J., 2020. Pollen-
628 based climate reconstruction techniques for late Quaternary studies. Earth-Science Reviews 103384.
629 Damsté, J.S.S., Hopmans, E.C., Pancost, R.D., Schouten, S., Geenevasen, J.A., 2000. Newly discovered non-isoprenoid glycerol dialkyl
630 glycerol tetraether lipids in sediments. Chemical Communications 1683–1684.
631 Davtian, N., Bard, E., Ménot, G., Fagault, Y., 2018. The importance of mass accuracy in selected ion monitoring analysis of branched and
632 isoprenoid tetraethers. Organic geochemistry 118, 58–62.
633 Davtian, N., Ménot, G., Bard, E., Poulenard, J., Podwojewski, P., 2016. Consideration of soil types for the calibration of molecular proxies for
634 soil pH and temperature using global soil datasets and Vietnamese soil profiles. Organic Geochemistry 101, 140–153.
635 https://doi.org/10.1016/j.orggeochem.2016.09.002
636 de Groot, W.J., Cantin, A.S., Flannigan, M.D., Soja, A.J., Gowman, L.M., Newbery, A., 2013. A comparison of Canadian and Russian boreal
637 forest fire regimes. Forest Ecology and Management 294, 23–34.
638 De Jonge, C., Radujković, D., Sigurdsson, B.D., Weedon, J.T., Janssens, I., Peterse, F., 2019. Lipid biomarker temperature proxy responds to
639 abrupt shift in the bacterial community composition in geothermally heated soils. Organic Geochemistry 137, 103897.
640 https://doi.org/10.1016/j.orggeochem.2019.07.006
641 De Jonge, C., Stadnitskaia, A., Hopmans, E.C., Cherkashov, G., Fedotov, A., Sinninghe Damsté, J.S., 2014. In situ produced branched glycerol
642 dialkyl glycerol tetraethers in suspended particulate matter from the Yenisei River, Eastern Siberia. Geochimica et Cosmochimica Acta
643 125, 476–491. https://doi.org/10.1016/j.gca.2013.10.031
644 Dearing Crampton-Flood, E., Tierney, J.E., Peterse, F., Kirkels, F.M.S.A., Sinninghe Damsté, J.S., 2020. BayMBT: A Bayesian calibration
645 model for branched glycerol dialkyl glycerol tetraethers in soils and peats. Geochimica et Cosmochimica Acta 268, 142–159.
646 https://doi.org/10.1016/j.gca.2019.09.043
647 Demske, D., Heumann, G., Granoszewski, W., Nita, M., Mamakowa, K., Tarasov, P.E., Oberhänsli, H., 2005. Late glacial and Holocene
648 vegetation and regional climate variability evidenced in high-resolution pollen records from Lake Baikal. Global and Planetary Change
649 46, 255–279. https://doi.org/10.1016/j.gloplacha.2004.09.020
650 Dole, R., Hoerling, M., Perlwitz, J., Eischeid, J., Pegion, P., Zhang, T., Quan, X.-W., Xu, T., Murray, D., 2011. Was there a basis for
651 anticipating the 2010 Russian heat wave? Geophysical Research Letters 38. https://doi.org/10.1029/2010GL046582
652 Drobyshev, I., Niklasson, M., Angelstam, P., 2004a. Contrasting tree-ring data with fire record in a pine-dominated landscape in the Komi
653 republic (Eastern European Russia): Recovering a common climate signal. Silva Fennica 38, 43–53.
654 Drobyshev, I., Niklasson, M., Angelstam, P., Majewski, P., 2004b. Testing for anthropogenic influence on fire regime for a 600-year period in
655 the Jaksha area, Komi Republic, East European Russia. Canadian Journal of Forest Research 34, 2027–2036.

Drotz, S.H., Sparrman, T., Nilsson, M.B., Schleucher, J., Öquist, M.G., 2010. Both catabolic and anabolic heterotrophic microbial activity proceed in frozen soils. Proceedings of the National Academy of Sciences 107, 21046–21051. https://doi.org/10.1073/pnas.1008885107

Druzhinina, O., Kublitskiy, Y., Stančikaitė, M., Nazarova, L., Syrykh, L., Gedminienė, L., Uogintas, D., Skipityte, R., Arslanov, K., Vaikutienė, G., Kulkova, M., Subetto, D., 2020. The Late Pleistocene–Early Holocene palaeoenvironmental evolution in the SE Baltic region: a new approach based on chironomid, geochemical and isotopic data from Kamyshovoye Lake, Russia. Boreas 49, 544–561. https://doi.org/10.1111/bor.12438

Dugerdil, L., Joannin, S., Peyron, O., Jouffroy-Bapicot, I., Vannière, B., Boldgiv, B., Unkelbach, J., Behling, H., Ménot, G., 2021. Climate reconstructions based on GDGT and pollen surface datasets from Mongolia and Baikal area: calibrations and applicability to extremely cold–dry environments over the Late Holocene. Climate of the Past 17, 1199–1226. https://doi.org/10.5194/cp-17-1199-2021

Feng, S., Hu, Q., Huang, W., Ho, C.-H., Li, R., Tang, Z., 2014. Projected climate regime shift under future global warming from multi-model, multi-scenario CMIP5 simulations. Global and Planetary Change 112, 41–52.

Fick, S.E., Hijmans, R.J., 2017. WorldClim 2: new 1-km spatial resolution climate surfaces for global land areas. International Journal of Climatology 37, 4302–4315. https://doi.org/10.1002/joc.5086

Foster, L.C., Pearson, E.J., Juggins, S., Hodgson, D.A., Saunders, K.M., Verleyen, E., Roberts, S.J., 2016. Development of a regional glycerol dialkyl glycerol tetraether (GDGT)–temperature calibration for Antarctic and sub-Antarctic lakes. Earth and planetary science letters 433, 370–379.

Girardin, M.P., Ali, A.A., Carcaillet, C., Blarquez, O., Hély, C., Terrier, A., Genries, A., Bergeron, Y., 2013. Vegetation limits the impact of a warm climate on boreal wildfires. New Phytologist 199, 1001–1011.

Glückler, R., Herzschuh, U., Kruse, S., Andreev, A., Vyse, S.A., Winkler, B., Biskaborn, B.K., Pestryakova, L., Dietze, E., 2020. Wildfire history of the boreal forest of southwestern Yakutia (Siberia) over the last two millennia documented by a lake-sedimentary charcoal record. Biogeosciences Discussions 1–42.

Goetz, S.J., Mack, M.C., Gurney, K.R., Randerson, J.T., Houghton, R.A., 2007. Ecosystem responses to recent climate change and fire disturbance at northern high latitudes: observations and model results contrasting northern Eurasia and North America. Environmental Research Letters 2, 045031.

Goldammer, J.G., 2015. Vegetation fires and global change-challenges for concerted international action: a white paper directed to the United Nations and International Organizations. Planet@ risk 3.

Goldammer, J.G., Furyaev, V.V., 1996. Fire in Ecosystems of Boreal Eurasia. Springer Netherlands, Dordrecht.

Goldammer, J.G., Sukhinin, A., Csiszar, I., 2005. The current fire situation in the Russian Federation: implications for enhancing international and regional cooperation in the UN framework and the global programs on fire monitoring and assessment. Int. Forest Fire News 32, 13–42.

Golubeva, Yu., 2008. Climate and vegetation of the Holocene in Komi Republic. (in Russian). Litosfera 124–132.

Grieser, J., Gommes, R., Bernardi, M., 2006. New LocClim-the local climate estimator of FAO. Geophys. Res. Abstr. 8.

Guiot, J., 1990. Methodology of the last climatic cycle reconstruction in France from pollen data. Palaeogeography, Palaeoclimatology, Palaeoecology 80, 49–69.

Harris, I., Jones, P. d., Osborn, T. j., Lister, D. h., 2014. Updated high-resolution grids of monthly climatic observations – the CRU TS3.10 Dataset. International Journal of Climatology 34, 623–642. https://doi.org/10.1002/joc.3711

Herzschuh, U., Böhmer, T., Chevalier, M., Dallmeyer, A., Li, C., Cao, X., Hébert, R., Peyron, O., Nazarova, L., Novenko, E.Y., Park, J., Rudaya, N.A., Schlütz, F., Shumilovskikh, L.S., Tarasov, P.E., Wang, Y., Wen, R., Xu, Q., Zheng, Z., 2022. Regional pollen-based Holocene temperature and precipitation patterns depart from the Northern Hemisphere mean trends. EGUsphere 1–23. https://doi.org/10.5194/egusphere-2022-127

Herzschuh, U., Böhmer, T., Li, C., Cao, X., 2021. Northern Hemisphere temperature and precipitation reconstruction from taxonomically harmonized pollen data set with revised chronologies using WA-PLS and MAT (LegacyClimate 1.0).

Hoegh - Guldberg, O., Jacob, D., Taylor, M., Bindi, M., Brown, S., Camilloni, I., Diedhiou, A., Djalante, R., Ebi, K., Engelbrecht, F., Guiot, K., Hijioka, Y., Mehrotra, S., Payne, A., Seneviratne, S., Thomas, A., Warren, R., Zhou, G., Halim, S., Achlatis, M., Alexander, L., Allen, M., Berry, P., Boyer, C., Brilli, L., Buckeridge, M., Cheung, W., Craig, M., Ellis, N., Evans, J., Fisher, H., Fraedrich, K., Fuss, S., Ganase, A., Gattuso, J., Greve, P., Guillen, T., Hanasaki, N., Hasegawa, T., Hayes, K., Hirsch, A., Jones, C., Jung, T., Kanninen, M., Krinner, G., Lawrence, D., Lenton, T., Ley, D., Liveman, D., Mahowald, N., McInnes, K., Meissner, K., Millar, R., Mintenbeck, K., Mitchell, D., Mix, A., Notz, D., Nurse, L., Okem, A., Olsson, L., Oppenheimer, M., Paz, S., Peterson, J., Petzold, J., Preuschmann, S., Rahman, M., Rogelj, J., Scheuffele, H., Schleussner, C.-F., Scott, D., Seferian, R., Sillmann, J., Singh, C., Slade, R., Stephenson, K., Stephenson, T., Sylla, M., Tebboth, M., Tschakert, P., Vautard, R., Wartenburger, R., Wehner, M., Weyer, N., Whyte, F., Yohe, G.,

Zhang, X., Zougmore, R., 2018. Chapter 3: Impacts of 1.5ºC global warming on natural and human systems, in: Global Warming of 1.5 °C an IPCC Special Report on the Impacts of Global Warming of 1.5 °C above Pre-Industrial Levels and Related Global Greenhouse Gas Emission Pathways, in the Context of Strengthening the Global Response to the Threat of Climate Change. Intergovernmental Panel on Climate Change.
Hopmans, E.C., Schouten, S., Damsté, J.S.S., 2016. The effect of improved chromatography on GDGT-based palaeoproxies. Organic Geochemistry 93, 1–6.
Hopmans, E.C., Weijers, J.W., Schefuß, E., Herfort, L., Damsté, J.S.S., Schouten, S., 2004. A novel proxy for terrestrial organic matter in sediments based on branched and isoprenoid tetraether lipids. Earth and Planetary Science Letters 224, 107–116.
Hu, F.S., Brubaker, L.B., Gavin, D.G., Higuera, P.E., Lynch, J.A., Rupp, T.S., Tinner, W., 2006. How climate and vegetation influence the fire regime of the Alaskan boreal biome: the Holocene perspective. Mitigation and Adaptation Strategies for Global Change 11, 829–846.
Huang, J., Zhang, X., Zhang, Q., Lin, Y., Hao, M., Luo, Y., Zhao, Z., Yao, Y., Chen, X., Wang, L., Nie, S., Yin, Y., Xu, Y., Zhang, J., 2017. Recently amplified arctic warming has contributed to a continual global warming trend. Nature Clim Change 7, 875–879. https://doi.org/10.1038/s41558-017-0009-5
Huguet, A., Fosse, C., Laggoun-Défarge, F., Delarue, F., Derenne, S., 2013. Effects of a short-term experimental microclimate warming on the abundance and distribution of branched GDGTs in a French peatland. Geochimica et Cosmochimica Acta 105, 294–315. https://doi.org/10.1016/j.gca.2012.11.037
Huguet, C., Hopmans, E.C., Febo-Ayala, W., Thompson, D.H., Damsté, J.S.S., Schouten, S., 2006. An improved method to determine the absolute abundance of glycerol dibiphytanyl glycerol tetraether lipids. Organic Geochemistry 37, 1036–1041.
Juggins, S., 2009. Package “rioja”–analysis of quaternary science data. The Comprehensive R Archive Network.
Juggins, S., Juggins, M.S., 2020. Package ‘rioja.’
Karmanov, V., Zaretskaya, N., Panin, A., Chernov, A., 2011. Reconstruction of local environments of ancient population in a changeable river valley landscape (The Middle Vychegda River, Northern Russia). Geochronometria 38, 128–137.
Kaufman, D., McKay, N., Routson, C., Erb, M., Dätwyler, C., Sommer, P.S., Heiri, O., Davis, B., 2020. Holocene global mean surface temperature, a multi-method reconstruction approach. Scientific data 7, 1–13.
Kharuk, V.I., Ponomarev, E.I., Ivanova, G.A., Dvinskaya, M.L., Coogan, S.C., Flannigan, M.D., 2021. Wildfires in the Siberian taiga. Ambio 1–22.
Klein Goldewijk, K., Beusen, A., Van Drecht, G., De Vos, M., 2011. The HYDE 3.1 spatially explicit database of human-induced global land-use change over the past 12,000 years. Global Ecology and Biogeography 20, 73–86.
Klimanov, V., 1976. To the method of reconstruction of quantitative parameters of past climate. Vestnik MGU Ser Geogr 2, 92–98.
Kultti, S., Väliranta, M., Sarmaja-Korjonen, K., Solovieva, N., Virtanen, T., Kauppila, T., Eronen, M., 2003. Palaeoecological evidence of changes in vegetation and climate during the Holocene in the pre-Polar Urals, northeast European Russia: HOLOCENE OF THE PRE-POLAR URALS. J. Quaternary Sci. 18, 503–520. https://doi.org/10.1002/jqs.765
Lapenis, A., Shvidenko, A., Shepaschenko, D., Nilsson, S., Aiyyer, A., 2005. Acclimation of Russian forests to recent changes in climate. Global Change Biology 11, 2090–2102.
Lau, W.K., Kim, K.-M., 2012. The 2010 Pakistan flood and Russian heat wave: Teleconnection of hydrometeorological extremes. Journal of Hydrometeorology 13, 392–403.
Li, X., Wang, M., Zhang, Y., Lei, L., Hou, J., 2017. Holocene climatic and environmental change on the western Tibetan Plateau revealed by glycerol dialkyl glycerol tetraethers and leaf wax deuterium-to-hydrogen ratios at Aweng Co. Quaternary Research 87, 455.
Loomis, S.E., Russell, J.M., Damsté, J.S.S., 2011. Distributions of branched GDGTs in soils and lake sediments from western Uganda: implications for a lacustrine paleothermometer. Organic Geochemistry 42, 739–751.
Loomis, S.E., Russell, J.M., Eggermont, H., Verschuren, D., Damsté, J.S.S., 2014. Effects of temperature, pH and nutrient concentration on branched GDGT distributions in East African lakes: Implications for paleoenvironmental reconstruction. Organic geochemistry 66, 25–37.
Marchenko-Vagapova, T.I., Marieva, N.A., 2001. Palynological and diatomic characteristics of environment in Holocene near middle Vychegda. Vestnik Institute of Geology. 2001. № 10. С. 6—9 6–9.
Marcott, S., Shakun, J., Clark, P., Mix, A., 2013. A Reconstruction of Regional and Global Temperature for the Past 11,300 Years. Science (New York, N.Y.) 339, 1198–201. https://doi.org/10.1126/science.1228026
Marsicek, J., Shuman, B.N., Bartlein, P.J., Shafer, S.L., Brewer, S., 2018. Reconciling divergent trends and millennial variations in Holocene temperatures. Nature 554, 92–96. https://doi.org/10.1038/nature25464

Martin, C., Menot, G., Thouveny, N., Peyron, O., Andrieu-Ponel, V., Montade, V., Davtian, N., Reille, M., Bard, E., 2020. Early Holocene Thermal Maximum recorded by branched tetraethers and pollen in Western Europe (Massif Central, France). Quaternary Science Reviews 228, 106109.

Matsueda, M., 2011. Predictability of Euro-Russian blocking in summer of 2010. Geophysical Research Letters 38.

Mauri, A., Davis, B., Collins, P., Kaplan, J., 2015. The climate of Europe during the Holocene: a gridded pollen-based reconstruction and its multi-proxy evaluation. Quaternary Science Reviews 112, 109–127.

Mayewski, P.A., Rohling, E.E., Curt Stager, J., Karlén, W., Maasch, K.A., Meeker, L.D., Meyerson, E.A., Gasse, F., van Kreveld, S., Holmgren, K., Lee-Thorp, J., Rosqvist, G., Rack, F., Staubwasser, M., Schneider, R.R., Steig, E.J., 2004. Holocene climate variability. Quat. res. 62, 243–255. https://doi.org/10.1016/j.yqres.2004.07.001

Moiseev, P., Bartysh, A., Nagimov, Z.Y., 2010. Climate changes and tree stand dynamics at the upper limit of their growth in the North Ural Mountains. Russian Journal of Ecology 41, 486–497.

Naafs, B., Inglis, G., Zheng, Y., Amesbury, M., Biester, H., Bindler, R., Blewett, J., Burrows, M., Del Castillo Torres, D., Chambers, F.M., 2017. Introducing global peat-specific temperature and pH calibrations based on brGDGT bacterial lipids. Geochimica et Cosmochimica Acta 208, 285–301.

Naeher, S., Peterse, F., Smittenberg, R.H., Niemann, H., Zigah, P.K., Schubert, C.J., 2014. Sources of glycerol dialkyl glycerol tetraethers (GDGTs) in catchment soils, water column and sediments of Lake Rotsee (Switzerland) – Implications for the application of GDGT-based proxies for lakes. Organic Geochemistry 66, 164–173. https://doi.org/10.1016/j.orggeochem.2013.10.017

Naryshkin, A.G., 2003. Fire and sustainable use of northern conifer forest in Russia. Presented at the Acta Horticulturae 615, IV International Conifer Conference 615, pp. 361–373.

Nazarova, L., Self, A.E., Brooks, S.J., van Hardenbroek, M., Herzschuh, U., Diekmann, B., 2015a. Northern Russian chironomid-based modern summer temperature data set and inference models. Global and Planetary Change 134, 10–25.

Nazarova, L., Self, A.E., Brooks, S.J., van Hardenbroek, M., Herzschuh, U., Diekmann, B., 2015b. Northern Russian chironomid-based modern summer temperature data set and inference models. Global and Planetary Change 134, 10–25.

Nedwell, D.B., 1999. Effect of low temperature on microbial growth: lowered affinity for substrates limits growth at low temperature. FEMS Microbiology Ecology 30, 101–111. https://doi.org/10.1111/j.1574-6941.1999.tb00639.x

Novenko, E., Olchev, A., 2015. Early Holocene vegetation and climate dynamics in the central part of the East European Plain (Russia). Quaternary International 388. https://doi.org/10.1016/j.quaint.2015.01.027

Pearson, E.J., Juggins, S., Talbot, H.M., Weckström, J., Rosén, P., Ryves, D.B., Roberts, S.J., Schmidt, R., 2011. A lacustrine GDGT-temperature calibration from the Scandinavian Arctic to Antarctic: Renewed potential for the application of GDGT-paleothermometry in lakes. Geochimica et Cosmochimica Acta 75, 6225–6238. https://doi.org/10.1016/j.gca.2011.07.042

Peterse, F., Nicol, G.W., Schouten, S., Damsté, J.S.S., 2010. Influence of soil pH on the abundance and distribution of core and intact polar lipid-derived branched GDGTs in soil. Organic Geochemistry 41, 1171–1175.

Peterse, F., van der Meer, J., Schouten, S., Weijers, J.W., Fierer, N., Jackson, R.B., Kim, J.-H., Damsté, J.S.S., 2012. Revised calibration of the MBT–CBT paleotemperature proxy based on branched tetraether membrane lipids in surface soils. Geochimica et Cosmochimica Acta 96, 215–229.

Peyron, O., Bégeot, C., Brewer, S., Heiri, O., Magny, M., Millet, L., Ruffaldi, P., Van Campo, E., Yu, G., 2005. Late-Glacial climatic changes in Eastern France (Lake Lautrey) from pollen, lake-levels, and chironomids. Quaternary Research 64, 197–211.

Peyron, O., Bordon, A., Vignot, A., Damy, S., Combourieu-Nebout, N., Brewer, S., Tarasov, P., Barboni, D., 2008. A modern pollen–climate database as a tool for quantitative climate and vegetation reconstructions, in: 12th International Palynological Congress IPC–XII. Bonn, Germany.

Peyron, O., Guiot, J., Cheddadi, R., Tarasov, P., Reille, M., de Beaulieu, J.-L., Bottema, S., Andrieu, V., 1998. Climatic reconstruction in Europe for 18,000 yr BP from pollen data. Quaternary research 49, 183–196.

Peyron, O., Magny, M., Goring, S., Joannin, S., de Beaulieu, J.-L., Bruggiapaglia, E., Sadori, L., Garfi, G., Kouli, K., Ioakim, C., 2013. Contrasting patterns of climatic changes during the Holocene across the Italian Peninsula reconstructed from pollen data.

Peyron, O., Simon, G., Isabelle, D., Ulrich, K., Jörg, P., Jacques-Louis, de B., Ruth, D.-S., Boris, V., Michel, M., 2011. Holocene seasonality changes in the central Mediterranean region reconstructed from the pollen sequences of Lake Accesa (Italy) and Tenaghi Philippon (Greece) [WWW Document]. URL https://journals.sagepub.com/doi/10.1177/0959683610384162 (accessed 9.12.22).

Ponel, P., Guiter, F., Gandouin, E., Peyron, O., Beaulieu, J.-L. de, 2022. Late-Glacial palaeotemperatures and palaeoprecipitations in the Aubrac Mountains (French Massif Central) reconstructed from multiproxy analyses (Coleoptera, chironomids and pollen). Quaternary International. https://doi.org/10.1016/j.quaint.2022.02.005

Pörtner, H.O., Roberts, D.C., Adams, H., Adler, C., Aldunce, P., Ali, E., Begum, R.A., Betts, R., Kerr, R.B., Biesbroek, R., 2022. Climate change 2022: impacts, adaptation and vulnerability.
Prentice, C., Guiot, J., Huntley, B., Jolly, D., Cheddadi, R., 1996. Reconstructing biomes from palaeoecological data: a general method and its application to European pollen data at 0 and 6 ka. Climate Dynamics 12, 185–194.
Ramos-Román, M.J., De Jonge, C., Magyari, E., Veres, D., Ilvonen, L., Develle, A.-L., Seppä, H., 2022. Lipid biomarker (brGDGT)- and pollen-based reconstruction of temperature change during the Middle to Late Holocene transition in the Carpathians. Global and Planetary Change 215, 103859. https://doi.org/10.1016/j.gloplacha.2022.103859
Raspopov, O., Lopatin, E., Kolström, T., Dergachev, V., Dmitriev, P., Kahle, H.-P., Spiecker, H., 2013. Spatial structure of periodicity in the conifer tree radial increment in the Republic of Komi. Izvestiya, Atmospheric and Oceanic Physics 49, 799–811.
Remy, C.C., Hély, C., Blarquez, O., Magnan, G., Bergeron, Y., Lavoie, M., Ali, A.A., 2017. Different regional climatic drivers of Holocene large wildfires in boreal forests of northeastern America. Environmental Research Letters 12, 035005.
Robles, M., Peyron, O., Brugiapaglia, E., Ménot, G., Dugerdil, L., Ollivier, V., Ansanay-Alex, S., Develle, A.-L., Tozalakyan, P., Meliksetian, K., 2022. Impact of climate changes on vegetation and human societies during the Holocene in the South Caucasus (Vanevan, Armenia): A multiproxy approach including pollen, NPPs and brGDGTs. Quaternary Science Reviews 277, 107297.
Ryzhkova, N., Kryshen, A., Niklasson, M., Pinto, G., Aleinikov, A., Kutyavin, I., Bergeron, Y., Ali, A.A., Drobyshev, I., 2022. Climate drove the fire cycle and humans influenced fire occurrence in the East European boreal forest. Ecological Monographs n/a, e1530. https://doi.org/10.1002/ecm.1530
Salonen, J.S., Ilvonen, L., Seppä, H., Holmström, L., Telford, R.J., Gaidamavičius, A., Stančikaitė, M., Subetto, D., 2012. Comparing different calibration methods (WA/WA-PLS regression and Bayesian modelling) and different-sized calibration sets in pollen-based quantitative climate reconstruction. The Holocene 22, 413–424.
Salonen, J.S., Seppä, H., Väliranta, M., Jones, V.J., Self, A., Heikkilä, M., Kultti, S., Yang, H., 2011. The Holocene thermal maximum and late-Holocene cooling in the tundra of NE European Russia. Quaternary Research 75, 501–511.
Sannikov, S., Goldammer, J., 1996. Fire ecology of pine forests of northern Eurasia, in: Fire in Ecosystems of Boreal Eurasia. Springer, pp. 151–167.
Schostag, M., Stibal, M., Jacobsen, C.S., Bælum, J., Taş, N., Elberling, B., Jansson, J.K., Semenchuk, P., Priemé, A., 2015. Distinct summer and winter bacterial communities in the active layer of Svalbard permafrost revealed by DNA- and RNA-based analyses. Frontiers in Microbiology 6.
Schubert, S., Wang, H., Suarez, M., 2011. Warm season subseasonal variability and climate extremes in the Northern Hemisphere: The role of stationary Rossby waves. Journal of Climate 24, 4773–4792.
Schubert, S.D., Wang, H., Koster, R.D., Suarez, M.J., Groisman, P.Y., 2014. Northern Eurasian heat waves and droughts. Journal of Climate 27, 3169–3207.
Schulze, E.-D., Wirth, C., Mollicone, D., Ziegler, W., 2005. Succession after stand replacing disturbances by fire, wind throw, and insects in the dark Taiga of Central Siberia. Oecologia 146, 77–88.
Seppä, H., Bjune, A.E., Telford, R.J., Birks, H., Veski, S., 2009. Last nine-thousand years of temperature variability in Northern Europe. Climate of the Past 5, 523–535.
Shorohova, E., Kuuluvainen, T., Kangur, A., Jõgiste, K., 2009. Natural stand structures, disturbance regimes and successional dynamics in the Eurasian boreal forests: a review with special reference to Russian studies. Annals of Forest Science 66, 1–20.
Sinopoli, G., Peyron, O., Masi, A., Holtvoeth, J., Francke, A., Wagner, B., Sadori, L., 2019. Pollen-based temperature and precipitation changes in the Ohrid Basin (western Balkans) between 160 and 70 ka. Climate of the Past 15, 53–71. https://doi.org/10.5194/cp-15-53-2019
Solovieva, N., Tarasov, P.E., MacDonald, G., 2005. Quantitative reconstruction of Holocene climate from the Chuna Lake pollen record, Kola Peninsula, northwest Russia. The Holocene 15, 141–148. https://doi.org/10.1191/0959683605hl793rr
Subetto, D.A., Nazarova, L.B., Pestryakova, L.A., Syrykh, L.S., Andronikov, A.V., Biskaborn, B., Diekmann, B., Kuznetsov, D.D., Sapelko, T.V., Grekov, I.M., 2017. Paleolimnological studies in Russian northern Eurasia: A review. Contemp. Probl. Ecol. 10, 327–335. https://doi.org/10.1134/S1995425517040102
Sun, Q., Chu, G., Liu, M., Xie, M., Li, S., Ling, Y., Wang, X., Shi, L., Jia, G., Lü, H., 2011. Distributions and temperature dependence of branched glycerol dialkyl glycerol tetraethers in recent lacustrine sediments from China and Nepal. Journal of Geophysical Research: Biogeosciences 116.
Tabatabai, M., Bailey, S., Bursac, Z., Tabatabai, H., Wilus, D., Singh, K.P., 2021. An introduction to new robust linear and monotonic correlation coefficients. BMC Bioinformatics 22, 170. https://doi.org/10.1186/s12859-021-04098-4

Tarasov, P., Bezrukova, E., Karabanov, E., Nakagawa, T., Wagner, M., Kulagina, N., Letunova, P., Abzaeva, A., Granoszewski, W., Riedel, F., 2007. Vegetation and climate dynamics during the Holocene and Eemian interglacials derived from Lake Baikal pollen records. Palaeogeography, Palaeoclimatology, Palaeoecology 252, 440–457.

Tarasov, P.E., Bezrukova, E.V., Krivonogov, S.K., 2009. Late Glacial and Holocene changes in vegetation cover and climate in southern Siberia derived from a 15 kyr long pollen record from Lake Kotokel. Clim. Past 11.

Tarasov, P.E., Guiot, J., Cheddadi, R., Andreev, A.A., Bezusko, L.G., Blyakharchuk, T.A., Dorofeyuk, N.I., Filimonova, L.V., Volkova, V.S., Zernitskaya, V.P., 1999. Climate in northern Eurasia 6000 years ago reconstructed from pollen data. Earth and Planetary Science Letters 171, 635–645. https://doi.org/10.1016/S0012-821X(99)00171-5

ter Braak, C.J., Juggins, S., 1993. Weighted averaging partial least squares regression (WA-PLS): an improved method for reconstructing environmental variables from species assemblages. Presented at the Twelfth International Diatom Symposium, Springer, pp. 485–502.

Tierney, J.E., Russell, J.M., Eggermont, H., Hopmans, E., Verschuren, D., Damsté, J.S., 2010. Environmental controls on branched tetraether lipid distributions in tropical East African lake sediments. Geochimica et Cosmochimica Acta 74, 4902–4918.

Tierney, J.E., Schouten, S., Pitcher, A., Hopmans, E.C., Damsté, J.S.S., 2012. Core and intact polar glycerol dialkyl glycerol tetraethers (GDGTs) in Sand Pond, Warwick, Rhode Island (USA): Insights into the origin of lacustrine GDGTs. Geochimica et Cosmochimica Acta 77, 561–581.

Tyler, J.J., Nederbragt, A.J., Jones, V.J., Thurow, J.W., 2010. Assessing past temperature and soil pH estimates from bacterial tetraether membrane lipids: evidence from the recent lake sediments of Lochnagar, Scotland. Journal of Geophysical Research: Biogeosciences 115.

Ulrich, M., Wetterich, S., Rudaya, N., Frolova, L., Schmidt, J., Siegert, C., Fedorov, A.N., Zielhofer, C., 2017. Rapid thermokarst evolution during the mid-Holocene in Central Yakutia, Russia. The Holocene 27, 1899–1913.

Velichko, A., Catto, N., Drenova, A., Klimanov, V., Kremenetski, K., Nechaev, V., 2002. Climate changes in East Europe and Siberia at the Late glacial–holocene transition. Quaternary International 91, 75–99.

Walker, X.J., Baltzer, J.L., Cumming, S.G., Day, N.J., Ebert, C., Goetz, S., Johnstone, J.F., Potter, S., Rogers, B.M., Schuur, E.A.G., Turetsky, M.R., Mack, M.C., 2019. Increasing wildfires threaten historic carbon sink of boreal forest soils. Nature 572, 520–523. https://doi.org/10.1038/s41586-019-1474-y

Wang, H., Liu, W., Zhang, C.L., Wang, Z., Wang, J., Liu, Z., Dong, H., 2012. Distribution of glycerol dialkyl glycerol tetraethers in surface sediments of Lake Qinghai and surrounding soil. Organic Geochemistry 47, 78–87.

Wang, L., Chen, W., Zhou, W., Chan, J.C., Barriopedro, D., Huang, R., 2010. Effect of the climate shift around mid 1970s on the relationship between wintertime Ural blocking circulation and East Asian climate. International Journal of Climatology: A Journal of the Royal Meteorological Society 30, 153–158.

Weijers, J., Wiesenberg, G.L., Bol, R., Hopmans, E., Pancost, R., 2010. Carbon isotopic composition of branched tetraether membrane lipids in soils suggest a rapid turnover and a heterotrophic life style of their source organism (s). Biogeosciences 7, 2959–2973.

Weijers, J.W., Bernhardt, B., Peterse, F., Werne, J.P., Dungait, J.A., Schouten, S., Damsté, J.S.S., 2011. Absence of seasonal patterns in MBT–CBT indices in mid-latitude soils. Geochimica et Cosmochimica Acta 75, 3179–3190.

Weijers, J.W., Schouten, S., Hopmans, E.C., Geenevasen, J.A., David, O.R., Coleman, J.M., Pancost, R.D., Sinninghe Damsté, J.S., 2006a. Membrane lipids of mesophilic anaerobic bacteria thriving in peats have typical archaeal traits. Environmental Microbiology 8, 648–657.

Weijers, J.W., Schouten, S., Sluijs, A., Brinkhuis, H., Damsté, J.S.S., 2007a. Warm arctic continents during the Palaeocene–Eocene thermal maximum. Earth and Planetary Science Letters 261, 230–238.

Weijers, J.W., Schouten, S., Spaargaren, O.C., Damsté, J.S.S., 2006b. Occurrence and distribution of tetraether membrane lipids in soils: Implications for the use of the TEX86 proxy and the BIT index. Organic Geochemistry 37, 1680–1693.

Weijers, J.W., Schouten, S., van den Donker, J.C., Hopmans, E.C., Damsté, J.S.S., 2007b. Environmental controls on bacterial tetraether membrane lipid distribution in soils. Geochimica et Cosmochimica Acta 71, 703–713.

Weijers, J.W., Schouten, S., van der Linden, M., van Geel, B., Sinninghe Damsté, J.S., 2004. Water table related variations in the abundance of intact archaeal membrane lipids in a Swedish peat bog. FEMS Microbiology Letters 239, 51–56.

Wohlfarth, B., Lacourse, T., Bennike, O., Subetto, D., Tarasov, P., Demidov, I., Filimonova, L., Sapelko, T., 2007. Climatic and environmental changes in north-western Russia between 15,000 and 8000calyrBP: a review. Quaternary Science Reviews 26, 1871–1883. https://doi.org/10.1016/j.quascirev.2007.04.005

Xiao, W., Wang, Y., Zhou, S., Hu, L., Yang, H., Xu, Y., 2016. Ubiquitous production of branched glycerol dialkyl glycerol tetraethers (brGDGTs) in global marine environments: a new source indicator for brGDGTs. Biogeosciences 13, 5883–5894. https://doi.org/10.5194/bg-13-5883-2016

Zaboeva, I.V., 1997. Soil ecology of Northern Taiga.

Zaretskaya, N.E., Panin, A.V., Golubeva, Y.V., Chernov, A.V., 2014. Sedimentation settings and the late pleistocene-holocene geochronology in the Vychegda River valley. Doklady Earth Sciences 455, 223–228. https://doi.org/10.1134/S1028334X14030118

Zink, K.-G., Vandergoes, M.J., Mangelsdorf, K., Dieffenbacher-Krall, A.C., Schwark, L., 2010. Application of bacterial glycerol dialkyl glycerol tetraethers (GDGTs) to develop modern and past temperature estimates from New Zealand lakes. Organic Geochemistry 41, 1060–1066.

913 **8. Supplementary Information**

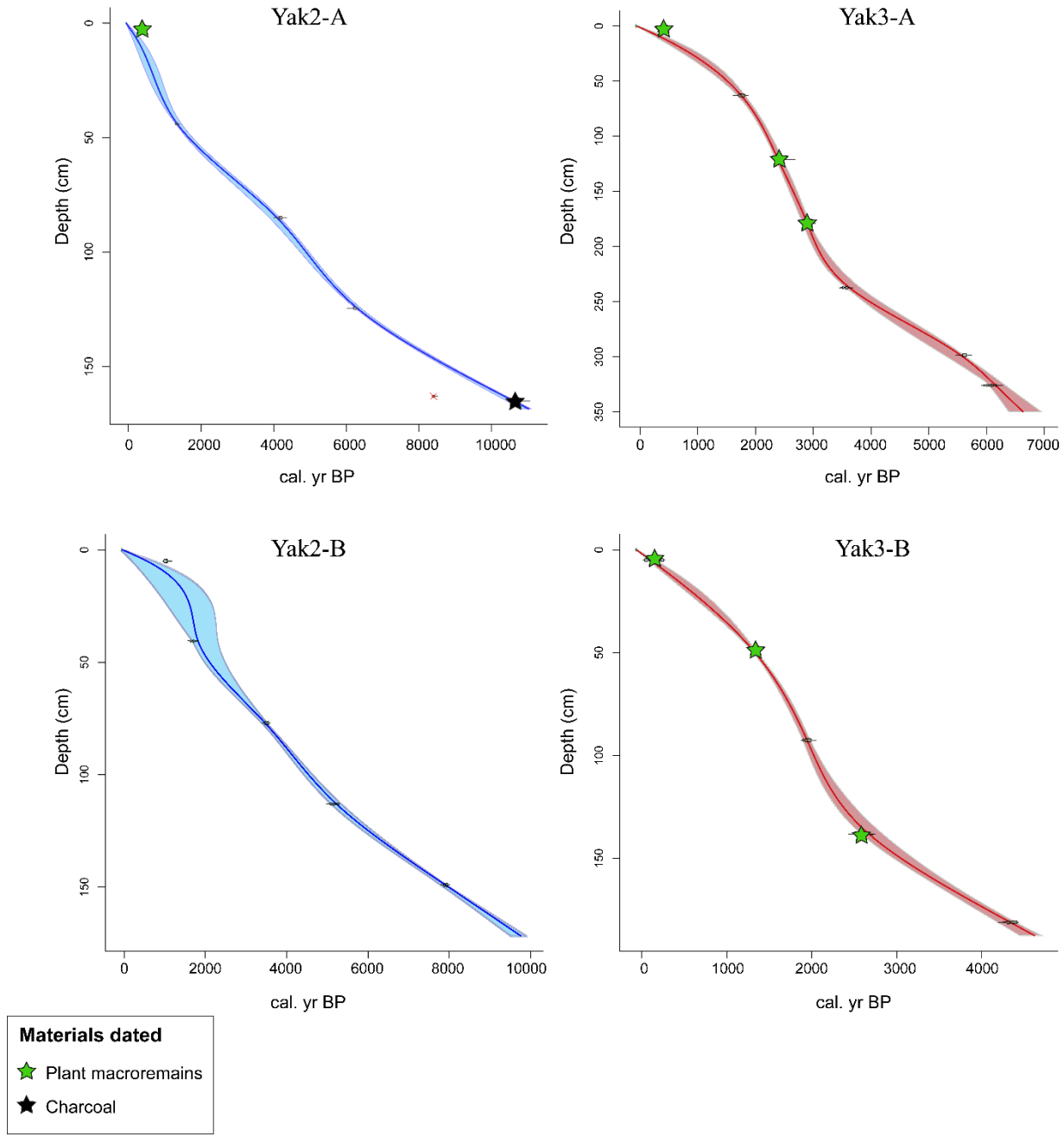

914

915 *SI 1: From Barhoumi et al. (2019): Age-depth model based on radiocarbon ages (see Table 2) from Yak2-A, Yak2-B, Yak3-A and Yak3-B cores.*
916 *The materials dated by 14C are bulk (single black lines), plant macroremains (green stars), macrocharcoal (black star).*

917

918

919

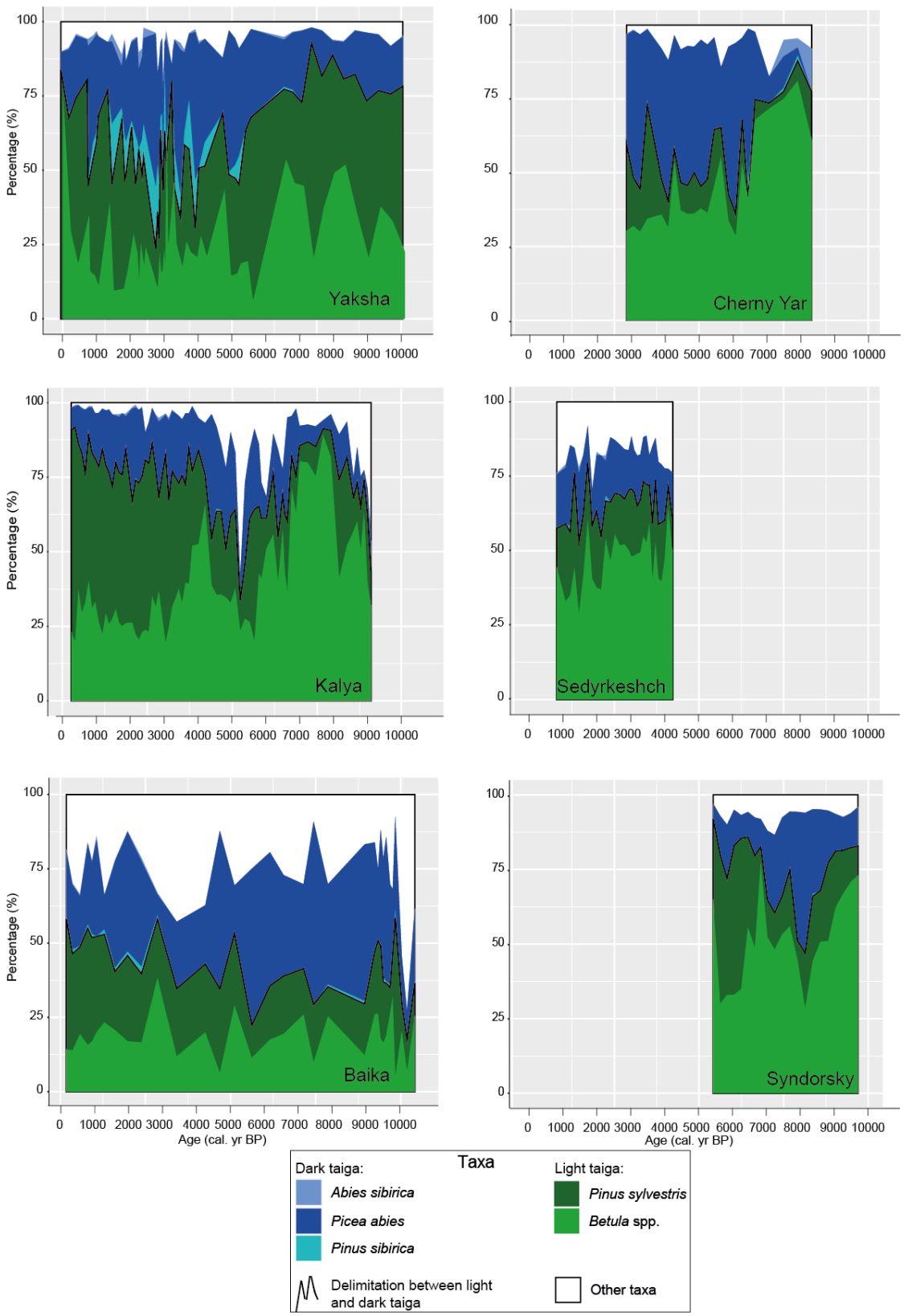

920

921 *SI 2: Cumulative pollen percentage diagram of principal taxa for each site: Yaksha, Baika, Kalya, Cherny Yar, Sedkyrkeshch and Syndorsky.*
922 *The main taxa shown are Betula spp. and Pinus sylvestris for the light taiga and Pinus sibirica, Picea abies and Abies sibirica for the dark taiga.*

923

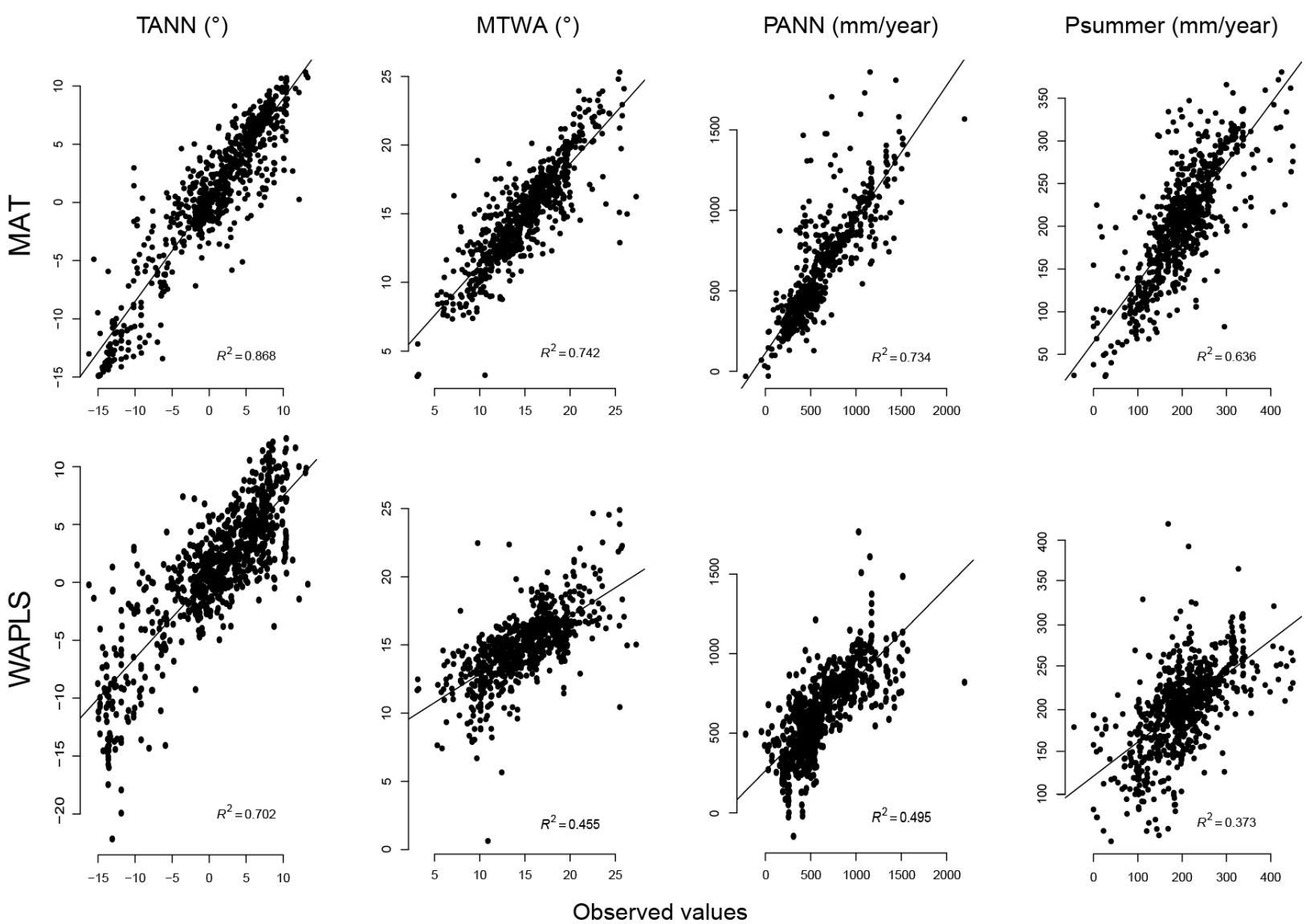

924

925 *SI 3: Correlations between the reconstructed values from the pollen transfer functions and the observed values of the randomly selected 40% of*
926 *the database*

927

928

929

930

931

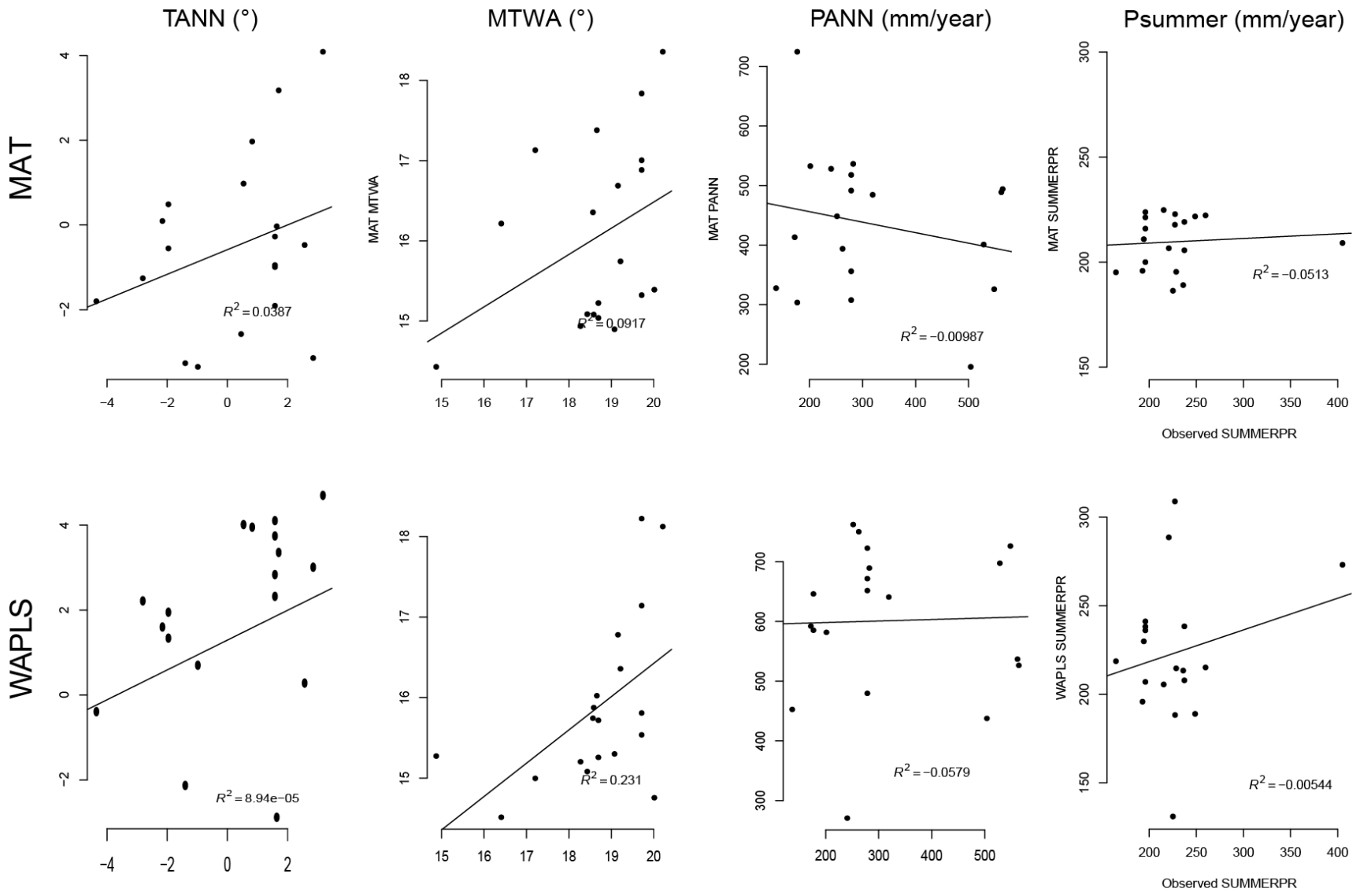

SI 4: Correlations between the reconstructed values from the pollen transfer functions and the observed values of the 19 samples situated between 40-50°N, 40-50°E of the database

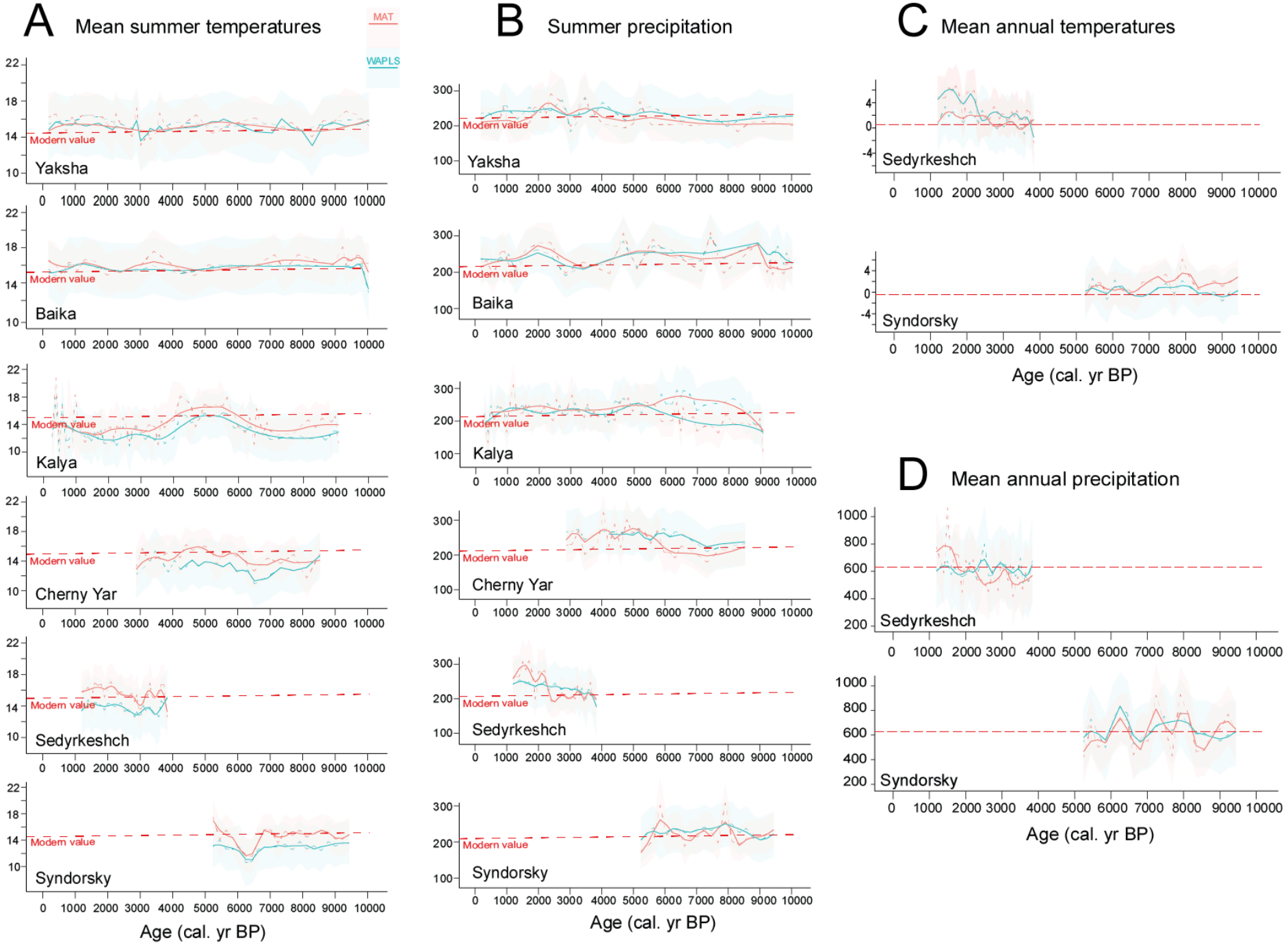
A
Mean summer temperatures
MAT
WAPLS
B
Summer precipitation
C
Mean annual temperatures
D
Mean annual precipitation
Modern value
Yaksha
Baika
Kalya
Cherny Yar
Sedyrkeshch
Syndorsky
Age (cal. yr BP)

*SI 5: Regional climatic synthesis of the Republic of Komi of pollen-based climatic reconstructions. Mean summer temperature (**A**), summer precipitation (**B**) and mean annual temperatures and precipitations (**C** and **D**) were calculated using the modern analogue technique (MAT) and the weighted average partial Least squares regression (WA-PLS) and smoothed using Loess (span = 0.3, solid lines). Shaded areas are confidence intervals. Red dashed lines are modern values for each site.*

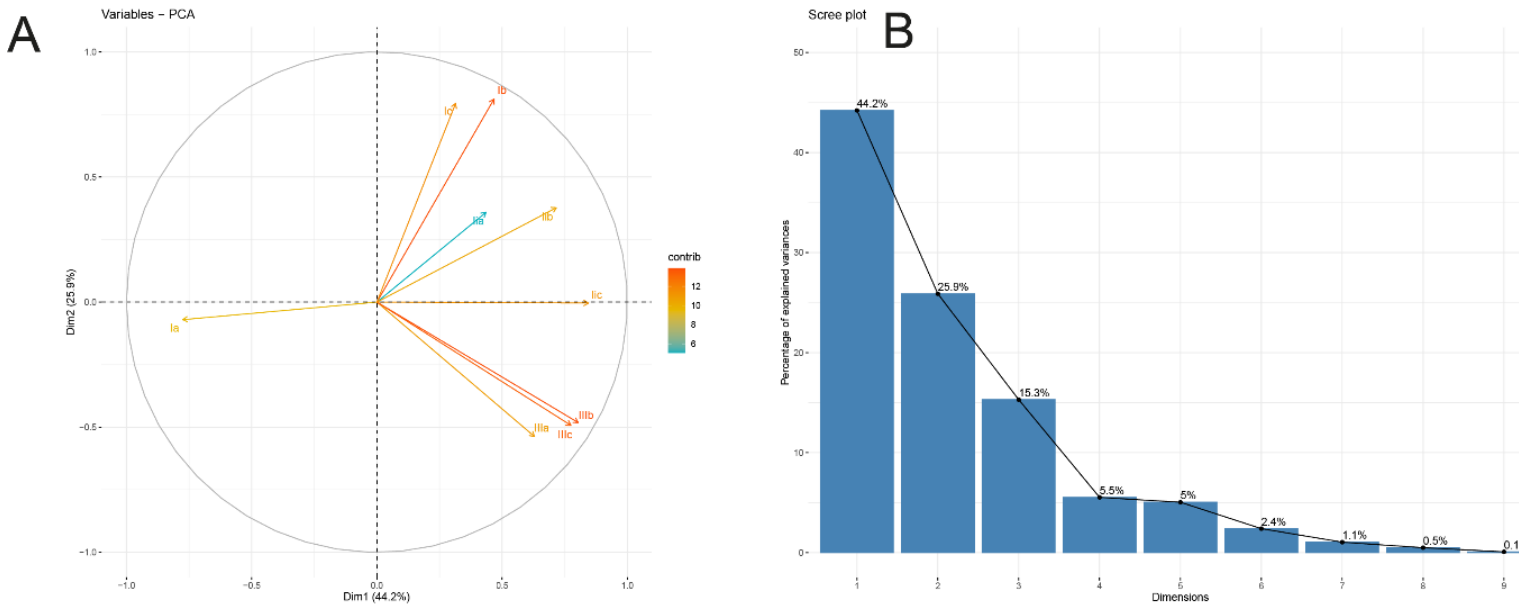

*SI 6: **A**: Yaksha brGDGTs PCA (axis 1 and axis 2). **B**: Yaksha brGDGTs PCA percentage of explained variances for each axis.*